DSTO

Comparison of Soot Model Predictions with Expermental Data for a Turbulent Sooting Propane Jet Flame.

Nigel S.A. Smith

DSTO-TR-0676

APPROVED FOR PUBLIC RELEASE

DEPARTMENT OF DEFENCE

DEFENCE SCIENCE AND TECHNOLOGY ORGANISATION

COMPARISON OF SOOT MODEL PREDICTIONS WITH EXPERIMENTAL DATA FOR A TURBULENT SOOTING PROPANE JET FLAME

Nigel S. A. Smith

Airframes and Engines Division
Aeronautical and Maritime Research Laboratory

DSTO–TR–0676

ABSTRACT

Simplified global reaction steps for soot particle formation, growth, oxidation and agglomeration have been incorporated into two separate models for turbulent nonpremixed combustion. The first of these models is a hybrid steady laminar flamelet (SLF) model which uses flamelet library data to determine the local rates of the aforementioned soot processes at various rates of strain and degrees of radiant heat loss. The second model employs the soot processes in a Conditional Moment Closure (CMC) method and solves for soot mass fraction and particle abundance concurrently with the determination of gas phase reactions and radiant heat loss. The predictions of these two models are compared with experimental data for a turbulent propane jet flame. It is found that the interdependence between the rate of soot processes and radiation losses is an integral feature of the modelling problem. In general, it was not possible to determine a universally appropriate set of soot process rates, due to the need to take differences in radiation heat loss submodels and turbulent combustion models into account.

DEPARTMENT OF DEFENCE

DEFENCE SCIENCE AND TECHNOLOGY ORGANISATION

Published by

DSTO Aeronautical and Maritime Research Laboratory
506 Lorimer St,
Fishermens Bend, Victoria, Australia 3207

Telephone: (03) 9626 7000
Facsimile: (03) 9626 7999

AR No. AR-010-557
August 1998

APPROVED FOR PUBLIC RELEASE

Comparison of soot model predictions with experimental data for a turbulent sooting propane jet flame

EXECUTIVE SUMMARY

The formation of soot and its impact upon radiation heat transfer from combustion systems and their hot exhausts is of critical significance to the maintenance and tactical effectiveness of modern military aircraft. Radiation from soot is the key heat transfer mechanism from combusting gases to surrounding solid surfaces in the hot section of gas turbine engines. The level and distribution of this heat transfer plays a determining role in the life of hot section components, most notably the combustor liner. Further, the presence of hot soot particles in the exhaust stream from an aircraft powerplant is thought to influence the nature of the infra-red signature of the aircraft, perhaps adding a substantial grey body emission source to the exhaust plume itself.

The purpose of DST Task 95/136 *Gas Turbine Combustor Modelling* has been to develop an in-house capability to numerically predict important characteristics in generic gas turbine combustion systems using a fundamentally sound, and therefore generally applicable, method. To date, soot modelling has been the primary focus of this task, as a result of its importance as outlined above. This report discusses the implementation of soot submodels, within existing well established models for turbulent nonpremixed combustion, at length.

In an earlier report (DSTO-TR-0631) by the author, titled *Comparison of CMC and SLF model predictions with experimental data for turbulent hydrogen jet flames*, the basic methodologies, advantages and disadvantages in the use of two advanced models for gas-phase nonpremixed turbulent combustion were described in detail. The earlier report described how the Conditional Moment Closure (CMC) model was implemented as a comprehensive post-processing step, available in addition to the Steady Laminar Flamelet (SLF) model in the commercial computational fluid dynamic package known as TASCflow3D. This report is a discussion of the means for, and results from, adding thermochemical processes for the nucleation, growth, oxidation and agglomeration of soot to these nominally gas-phase models.

The basis for validation of the new soot-capable models is through comparison with experimental data taken from the literature for a turbulent nonpremixed propane jet flame. Jet flames are frequently used in model validation due to their reproducibility, accessibility for measurement, and because they possess a flow field which is relatively straightforward to compute. The comparison of model predictions with jet flame measurements in this report shows that the predictions of a single soot thermochemical mechanism is markedly different depending on a) which turbulent combustion model it is implemented within, and b) which radiation loss model is employed. Much of the discussion presented in this report focuses on the understanding of the different predictions offered by each model, and practices that should be adopted in employing these models in the future, in combustor-like flows.

THIS PAGE IS INTENTIONALLY BLANK

Author

Nigel S. A. Smith
Airframes and Engines Division

Nigel Smith completed a Bachelor of Engineering with Honours (Mechanical) at the University of Western Australia in 1990. His honours dissertation was a study of flow modification in flat-plate turbulent boundary layers as a result of riblet surface modifications, using laser doppler velocimetry.

Between 1991 and 1994, he studied towards a Ph.D. at the University of Sydney, in the Department of Mechanical Engineering. His research dealt with the development and testing of the Conditional Moment Closure method for predicting turbulent combustion processes. Along the way, he was able to travel and work extensively at the Combustion Research Facility at Sandia National Laboratories in Livermore, California, as well as at Cambridge University and the NATO Advanced Study Institute Workshop in Les Houches, France.

Upon completion of his Ph.D. research and thesis in September of 1994, he took up a position as a postdoctoral fellow at the Center for Turbulence Research, a joint research facility operated by Stanford University and the NASA Ames Research Center. After two years of research into turbulent combustion using direct numerical simulation, he found his way back from Northern California to Melbourne, where he has taken up an RS position in the Airframes and Engines Division.

Nigel Smith's current research objective is to provide DSTO with a credible in-house capability for the prediction of turbulent combustion dynamics in a generic gas turbine combustor setting. The successful implementation of this capability will allow DSTO to better serve the future needs of its customer as they arise, rather than after the fact.

THIS PAGE IS INTENTIONALLY BLANK

Contents

THIS PAGE IS INTENTIONALLY BLANK

1 Introduction

In order to numerically predict the nature and effect of turbulent nonpremixed combustion in gas turbine engine combustors (GTCs) an integrated model framework, consisting of many different component models, is typically required. Examples of these component models include methods for predicting the dynamics of turbulent flow, the relationship between gas-phase combustion processes and fluid mixing, the magnitude and distribution of radiated heat transfer, and the dynamics of solid and liquid -phase interaction with the gas phase. A number of component models have been discussed in an earlier report[1]; principally those concerned with gas-phase combustion interaction with fluid mixing, and radiant heat transfer. The scope of this particular investigation is the development, implementation and testing of component models for solid phase dynamics in turbulent nonpremixed combustion.

A feature of the combustion of hydrocarbon fuels in air is the formation and destruction of small solid carbonaceous particles, known as soot, within the combustion zone. These tiny amorphous particles range in size from a few nanometres to many micrometres in terms of characteristic width, and have a varied composition commonly consisting of carbon, hydrogen, oxygen, and other elements which are dependent on the nature of the fuel being burnt.

The presence of soot particles in a flame has a profound influence on the nature and level of radiant heat transfer from that flame and thus the temperature and structure of the reaction zones themselves. Radiation from soot particles tends to closely approximate greybody emission, and the associated degree of heat loss is typically much greater than arising from narrow band emitting gaseous species like carbon dioxide (CO_2) and water (H_2O). The presence of soot in flames is easily confirmed with the naked eye; their greybody emission is responsible for the characteristic yellow-orange colouration that is popularly associated with flames and fire. The accurate prediction of soot levels in practical combustion systems is a determining factor in the correct estimation of radiant heat transfer from the reaction zones to cooler surrounds. Conversely, the highly temperature-sensitive nature of soot formation means that the accurate determination of radiant heat losses is critical in determining the levels of soot likely to be present.

Soot particles form in fuel rich zones of fluid where temperatures are still high. After inception, soot particles are subject to three separate and distinct mass and number density altering processes. Existing soot particles act as sites for further deposition of hot fuel-rich material, causing an increase in surface area and particle mass while not in itself leading to a greater number of particles. In addition, soot particles that exist in the presence of strong oxidizing agents are subject to the oxidation and removal of deposited material, which results in a surface area and mass decrease. Finally, it is known that soot particles tend to agglomerate as a result of chance collisions between one another. This process of agglomeration does not increase the mass of soot present, but reduces the overall number of particles, and thus the mass per particle. The rates of soot particle inception, surface growth and surface oxidation are all thought to be strong functions of local temperature and the concentrations of gaseous oxidants and high-carbon bearing species.

Based on this simplified understanding of soot particle dynamics, a soot model has been adopted and incorporated with two turbulent combustion models (Steady Laminar

Flamelet - SLF, and Conditional Moment Closure - CMC) into an implementation for a general-purpose computational fluid dynamics code. This report describes the nature of the soot model, how it is incorporated into the SLF and CMC models, and the issues surrounding this implementation as functional code.

Preliminary results for soot predictions compared with the experimental measurements of Nishida and Mukohara[2], for a turbulent propane jet diffusion flame at atmospheric pressure.

2 Method

In reality, the soot field generated by hydrocarbon combustion contains a wide distribution of sizes, shapes, densities, and compositions of soot particles[3]. In the derivation of appropriate soot models, simplifying assumptions will be made in relation to all of these particle properties. These assumptions will be introduced where necessary.

Smaller lighter soot particles tend to follow local fluid motion closely, while larger more massive soot particles follow trajectories that are far smoother than those of surrounding fluid *parcels*. Due to the tendency for some particles to follow inertially determined trajectories instead of tracking the flow, it is reasonable to expect that only a Lagrangian methodology will be successful in describing soot motion. While this is possible, if the contribution of very large soot particles to the overall soot field is small, then it is computationally expedient to represent soot particle dynamics in an Eulerian frame instead.

Equations can be derived for the local instantaneous transport and evolution of field variables describing soot characteristics at fixed points in space and time. The most obvious such variable is soot mass fraction (Y_s), which denotes the ratio of the mass of soot present at the sample point to the total mass present. The equation for soot mass fraction is given by,

$$\frac{\partial Y_s}{\partial t} + u_i \frac{\partial Y_s}{\partial x_i} = -\frac{\partial}{\partial x_i}\left(u_{i,T} Y_s\right) + \dot{w}_{s,Y} \ , \tag{1}$$

where u_i denotes the local fluid velocity component in the ith direction, $u_{i,T}$ denotes the particle velocity component due to thermophoresis, and $\dot{w}_{s,Y}$ denotes the net rate of chemical production of soot mass from gaseous surroundings.

At least one other variable is required in order to represent a field of variably sized particles, namely some measure of the number of particles present. Since soot particles are present in any number of sizes in any given sample, there should ideally be a variable provided for each size *class*. In this representation, however, it is assumed that all soot particles in any given sample are of the same size. Note that this does not restrict particle sizes from varying between samples. The number of moles of soot particles per unit mass of mixture is therefore given by,

$$\frac{\partial \Gamma_s}{\partial t} + u_i \frac{\partial \Gamma_s}{\partial x_i} = -\frac{\partial}{\partial x_i}\left(u_{i,T} \Gamma_s\right) + \dot{w}_{s,\Gamma} \ , \tag{2}$$

where $\dot{w}_{s,\Gamma}$ is the net rate of soot particle formation as a result of chemistry and particle-particle interaction.

Equations (1) & (2) bear some similarity to the equations for the local instantaneous evolution of gaseous species. In the case of a gaseous species, however, molecular structure dictates a fixed relationship between the mass fraction of the species (Y_i), and its molar abundance (Γ_i), through the molecular weight (W_i). There is no such relationship for soot particles, which can instead have any number of constituent molecules or atoms above an arbitrary 'inception' value.

Note that equations (1) & (2) do not contain the familiar molecular diffusion terms associated with gaseous species, and instead contain a dispersive term due to thermophoretic motion. Even finely divided solid particles like soot, do not diffuse appreciably in comparison to gaseous molecules, which are very much smaller again. Thermophoresis is the tendency for small particles to move in the direction of decreasing local temperature. Due to their substantial size on a molecular level, soot particles are subject to differential heating by their gaseous surroundings, which leads to differing rates of mass and momentum exchange with the particle surface. These differential rates across the surface of a single particle produce a small net thrust on the particle, resulting in thermophoretic motion.

Knowledge of soot mass fraction and particle molar abundance in a sample can be used to determine other important quantities which are relevant to the thermochemical dynamics of soot particles. The volume occupied by each soot particle (v_p) can be expressed in terms of the local mass fraction of soot (Y_s), and the local particle molar abundance (Γ_s), as

$$v_p = \frac{Y_s}{\rho_p \Gamma_s N_A} \ . \tag{3}$$

In the above, the material density of soot particles (assumed uniform for all particles) is denoted by ρ_p, and Avogadro's Number is denoted by N_A. A value of 2000 kilograms per cubic metre has been adopted throughout this study as the material density of all soot particles. If it is assumed that the soot particles have a fixed regular shape, then it is possible to relate a characteristic particle diameter (d_p) and surface area (s_p) to the computed particle volume v_p. In the case of spherical particles these relations are given by

$$d_p = \left(\frac{6v_p}{\pi}\right)^{1/3} \ , \ s_p = \pi d_p^2 \ . \tag{4}$$

The amount of surface area of soot per unit volume of mixture (S) is an important quantity in the calculation of the surface chemistry which occurs at the solid-gas interface. Surface area per unit volume can be expressed in terms of the soot mass fraction and particle molar abundance as,

$$S = s_p \rho \Gamma_s N_A = C_s \rho Y_s^{2/3} \Gamma_s^{1/3} \tag{5}$$

where the constant C_s has the following definition for spherical particles,

$$C_s \equiv (\pi N_A)^{1/3} \left(\frac{6}{\rho_p}\right)^{2/3} \ . \tag{6}$$

2.1 Modelled rates of soot processes

The principal difficulty encountered in the use of equations (1) & (2) is the closure of the chemically-based source terms ($\dot{w}_{s,Y}$, $\dot{w}_{s,\Gamma}$). There is reasonably wide agreement that

Process Step	Rate coefficient (A)	Temperature Index	Activation Temperature (Θ)
Nucleation	1.0×10^4	0.0	21100
Surface Growth	1.2×10^4	0.0	12100
Oxidation (O_2)	7.15×10^2	0.5	19680
Oxidation (OH)	2.51×10^5	0.5	0.0

Table 1: Arrhenius rate expressions for modelled soot reactions, taken largely from ref. 6. Rate coefficients (A) are subject to alteration in this study. All constants are given in the appropriate SI *units.*

their are four basic soot-related processes at work, potentially simultaneously, in sooting flames[3, 4].

These processes of nucleation, surface growth, oxidation and agglomeration appear in the source terms for equations (1) & (2) as,

$$\dot{w}_{s,Y} = W_C \left(r_{nucl} + r_{grow} - r_{oxid} \right) \ , \tag{7}$$

and

$$\dot{w}_{s,\Gamma} = 2 r_{nucl} N_{incip}^{-1} - r_{aggl} \ , \tag{8}$$

where N_{incip} is the number of carbon atoms in an incipient soot particle. Leung *et al.*[5] employ an incipient value of $N_{incip} = 100$; this value is also employed in this study.

The following describes a modelling methodology, similar to that employed by Jones, Lindstedt and coworkers[5, 6], which has been adopted in this study to represent each of the processes : r_{nucl}, r_{grow}, r_{oxid} and r_{aggl}.

The steps corresponding to nucleation, surface growth, and oxidation are described using Arrhenius expressions, consisting of the product of a rate coefficient, temperature raised to a constant power index, and the exponent of an activation temperature divided by the local temperature. The value of the constants in these expressions used in the past [5, 6] is given in Table 1. The value of the rate coefficients in each case was determined largely by the predicted results in the jet flames studied [5, 6]. As a result, the tabulated values of these coefficients will have depended on non-chemical aspects of the overall flame predictions, such as radiation heat loss. It will be seen later that different values of the rate coefficient must be selected in this case to account for the improved radiation heat loss model employed in this study.

2.1.1 Soot nucleation

The actual mechanics behind the formation of solid soot particles from a combusting gaseous mixture are not well understood. It is generally accepted that the presence of high levels of intermediate pyrolysis and oxidation products, particularly acetylene (C_2H_2) and unsaturated aromatic hydrocarbons, is closely associated with the nucleation of soot particles[3]. However, the exact nature of any progression from these carbon-rich species to long chain polyacetylenes and polycyclic aromatics, and on to solid nuclei, possibly via a meta-stable liquid phase, still defies detailed description.

In the place of an actual understanding of the nucleation of soot, models have been devised to correlate rates of particle inception with temperature and the concentration of C_2H_2 or an aromatic hydrocarbon such as benzene (C_6H_6). Leung *et al.*[5] provide one such semi-empirical fit for soot nucleation and initial surface growth. Expressed in a traditional Arhenius form, the fit is given below in terms of local temperature (T), and local acetylene molar abundance (Γ_{C2H2}),

$$r_{nucl} = k_{nucl}\Gamma_{C2H2} \ , \ k_{nucl} = A_{nucl}e^{-\Theta_{nucl}/T} \tag{9}$$

where Θ_{nucl} is the activation temperature for the reaction, and A_{nucl} is the corresponding rate coefficient.

2.1.2 Soot surface growth

Unlike particle inception, the continued growth of existing particles is a function of the amount of surface area available for further reaction. This area dependence is not linear as one might expect, but seems best fitted with experiment when a half-power law is adopted in order to account for decreased surface reactivity on larger older particles[5]. The dependence of soot growth upon the presence of soot precursors (C_2H_2), is modelled as being similar to the dependence in the case of nucleation. The rate of soot mass accumulation through surface growth is somewhat slower than the build-up associated with nucleation and early growth[5]. However, the overwhelming bulk of mass addition occurs through surface growth. The modelled expression for surface growth is given as,

$$r_{grow} = k_{grow}S^{1/2}\Gamma_{C2H2} \ , \ k_{grow} = A_{grow}e^{-\Theta_{grow}/T} \tag{10}$$

where S denotes the surface area of soot per unit volume of mixture.

2.1.3 Soot oxidation

Oxidation of soot occurs at the particle surface, and is a function of temperature, and the local concentrations of oxidizers such as oxygen (O_2) and hydroxyl radical (OH). Various studies have shown that the significance of these two oxidants varies according to the local levels of temperature and other species[7, 8], as well as soot structure[9].

Leung *et al.*[5] employ a solely oxygen-based expression to model soot oxidation, despite the reported[10] significance of oxidation by OH. In this study, various oxidation rate expressions have been employed, including that of Leung *et al.*[5], and one which involves oxidation by OH. In both cases, a linear dependence on surface area per unit volume is present. The total oxidation rate is given by,

$$r_{oxid} = S\left(k_{ox1}\Gamma_{O2} + k_{ox2}\Gamma_{OH}\right) \tag{11}$$

where the component reaction expressions are given by,

$$k_{ox1} = A_{ox1}T^{1/2}e^{-\Theta_{ox1}/T} \ , \ k_{ox2} = A_{ox2}T^{1/2} \tag{12}$$

2.1.4 Soot agglomeration

The collision of soot particles frequently results in the adherence of the colliders. This agglomeration of soot particles leads to a fewer number of soot particles, but with each particle carrying more mass. The rate at which agglomeration occurs is given by a well known relationship[3],

$$r_{aggl} \equiv 2C_{aggl}N_A\left(\frac{6d_p\kappa T}{\rho_p}\right)^{1/2}(\rho\Gamma_s)^2 \ , \tag{13}$$

where C_{aggl} is a constant (9.0) , N_A is Avogadro's number, and κ is the Boltzmann constant.

Apart from nucleation and agglomeration, no other processes have an effect upon the particle molar abundance (Γ_s). In reality it is conceivable that oxidation may completely eliminate soot particles, however this effect is not accounted for. Instead, the number of particles is unaffected by oxidation, while the mass of these particles can tend to zero.

2.2 Soot modelling in turbulent flow

The soot model described in the preceeding section applies only for computations that are fully spatially and temporally resolved down to the smallest scales of motion. To apply this model in a turbulent flow, at a correspondingly coarser level of resolution, the model equations must be appropriately averaged. This is precisely the same procedure which is performed in deriving the averaged equations for gas phase combustion from their local and instantaneous origins[1].

The Favre averaged equations for mean soot mass fraction ($\langle Y_s\rangle$) and mean particle molar abundance ($\langle\Gamma\rangle$) can be written as,

$$\frac{\partial\langle Y_s\rangle}{\partial t} + \langle u_i\rangle\frac{\partial\langle Y_s\rangle}{\partial x_i} = -\frac{\partial}{\partial x_i}\left(\langle u_i' y_s\rangle\right) + \langle\dot{w}_{s,Y}\rangle \ , \tag{14}$$

$$\frac{\partial\langle\Gamma_s\rangle}{\partial t} + \langle u_i\rangle\frac{\partial\langle\Gamma_s\rangle}{\partial x_i} = -\frac{\partial}{\partial x_i}\left(\langle u_i'\gamma_s\rangle\right) + \langle\dot{w}_{s,\Gamma}\rangle \tag{15}$$

where u_i' is the fluctuating part of the turbulent velocity component in the ith direction, and y_s and γ_s are the fluctuating parts of soot mass fraction and particle molar abundance respectively. Note that the equations neglect the influence of thermophoresis, since its effect is likely to be very much less than the dispersion of particles arising out of the turbulent transport terms $\frac{\partial}{\partial x_i}\left(\langle u_i' y_s\rangle\right)$ and $\frac{\partial}{\partial x_i}\left(\langle u_i'\gamma_s\rangle\right)$. This turbulent transport can be modelled using any of the standard techniques, including $k-\epsilon$ modelling (via a gradient transport assumption) and second order closure methods.

As with modelling gas phase combustion in a turbulent environment[1], the crux of the modelling problem in equations (14) & (15) lies with the closure of the *averaged* chemical source terms ($\langle\dot{w}_{s,Y}\rangle$, $\langle\dot{w}_{s,\Gamma}\rangle$). Due to the highly non-linear nature of chemical source terms, closure of their means cannot be effected by evaluating their instantaneous expressions using averaged quantities.

$$\langle\dot{w}_s(Y_s,\Gamma_s,T,\ldots)\rangle \neq \dot{w}_s(\langle Y_s\rangle,\langle\Gamma_s\rangle,\langle T\rangle,\ldots) \tag{16}$$

A tremendous body of research exists for the treatment of this problem for gas-phase turbulent nonpremixed combustion[1]. Many of the lessons learned in that arena can be readily applied to the problem for soot chemistry. Two modified gas-phase models, suitable for soot prediction have been selected for further development. The details of these two models are described below.

2.2.1 Sootlet hybrid model

The Steady Laminar Flamelet (SLF) method has been shown to have significant versatility in the prediction of gas phase turbulent nonpremixed phenomena[11, 12]. In using this method, the assumption is made that all combustion reactions occur on time and length scales that are substantially smaller than the those of the mixing processes in which the combustion occurs. Under these conditions, parameterised laminar flame data can be used to represent the thermochemical structure of turbulent flames.

Some of the great advantages of the SLF method are that it is computationally inexpensive, and numerically robust in its application. It does, however, have several notable drawbacks[1]; some of these preclude its direct application to soot prediction. Since soot formation occurs on timescales which are long compared to the timescales of local mixing of fuel and oxidizer, soot cannot be treated as a species which is confined to thin laminar flamelet structures. Furthermore, the significant degree of radiant heat loss associated with soot formation causes a progressive depletion of sensible enthalpy with residence time for the hot fluid within the combustion system. The timescale of this energy depletion is also much larger than the timescales of local mixing, and so cannot be represented using a steady laminar flamelet methodology.

Fairweather *et al.*[6] proposed a hybrid scheme whereby the gaseous species of the combustion system are treated using a traditional SLF method, while the soot mass fraction and particle molar abundance are computed separately. The averaged source terms for the soot variables were determined in two parts. Firstly, those portions of the source terms which could be evaluated locally and instantaneously using flamelet data were stored in a companion library. Secondly, during the actual calculation of the soot fields, averaged soot mass fractions and particle molar abundances were used to complete the source term evaluation.

Thus the following partial closure of the averaged source equations (9 - 13) was effected; one which does not account for correlations between the soot variables and the gas phase species and temperature.

$$\langle r_{nucl} \rangle = \langle k_{nucl} \Gamma_{C2H2} \rangle \tag{17}$$

$$\langle r_{grow} \rangle \approx \langle k_{grow} \Gamma_{C2H2} \rangle \langle S \rangle^{1/2} \tag{18}$$

$$\langle r_{oxid} \rangle \approx \left(\langle k_{ox1} \Gamma_{O2} \rangle + \langle k_{ox2} \Gamma_{OH} \rangle \right) \langle S \rangle \tag{19}$$

$$\langle r_{aggl} \rangle \approx \langle 2 C_{aggl} N_A \sqrt{\frac{6\kappa T}{\rho_p}} \rangle \langle \rho \rangle^2 \langle \Gamma_s \rangle^2 \langle d_p \rangle^{1/2} \tag{20}$$

Fairweather *et al.*[6] employed a heuristic approach in dealing with the influence of radiant heat losses on the flame structure and consequent soot formation behaviour. A

radiation factor (β) was applied to the temperature profiles of a steady adiabatic strained laminar diffusion flame of propane in air,

$$T = T_{ad}\left(1 - \beta\left(\frac{T_{ad}}{\hat{T}_{ad}}\right)^4\right) \quad . \tag{21}$$

In the above, T_{ad} denotes an adiabatic temperature taken anywhere on the profile, $\hat{T}_{ad}$ denotes the peak adiabatic temperature on the profile, and T denotes the *modified* temperature used in computing soot reaction rates.

The intention of this *a priori* modification was to mimic a temperature profile which might arise through radiant losses. By tuning the constant β, Fairweather *et al.*[6] demonstrated that it was possible to produce temperatures of an appropriate magnitude throughout the bulk of their modelled flame. Reasonable agreement between soot predictions, based on these modified temperatures, and experimental data was subsequently found.

A number of objections to this approach can be raised in connection with its broader use. Firstly, by using a constant value of the radiation factor (β) throughout the entire flame, a significant qualitative difference is introduced between the observed temperature profiles in sooting flames and that predicted by Fairweather *et al.* Unlike what occurs in reality, the model gives no indication of the progressive radiant heat loss throughout the flame. Instead, if given the same mixing state at two widely separated measurement stations, the model would predict identical temperatures. Secondly, while the *a priori* selection of an appropriate radiation factor in a turbulent jet flame might be relatively simple, albeit entirely empirical, there is no indication that this process will be quite so straight forward in a more complex flow geometry.

In the course of this investigation, the source term closure of Fairweather *et al.* was adopted, but with some notable differences in relation to the treatment of radiation loss. Instead of generating a single library of reaction rate data, using a selected radiation factor and modified temperature profile, a large number of libraries (15) were generated to cover a wide range in radiation factor ($-0.1 \leq \beta \leq 0.45$). These various libraries were used in conjunction with the radiant heat transfer calculations built into the CFD code. At each point in the calculation, the local temperature was free to vary according to radiant heat loss, sensible heat evolution through chemical reaction, and convective cooling. These local temperatures were used to identify the appropriate library of soot reaction rate data, at each point, through a comparison with the library-tabulated temperatures for the given local mixing state. In contrast to the methodology of Fairweather *et al.*, the practice described above does not arbitrarily pre-determine an appropriate value of β, but allows for a radiation-driven progression in β throughout the combustion system. Two different schemes for modelling radiation loss were trialled in conjunction with this method, namely optically-thin and optically-thick approximations. These radiation schemes are discussed in Section 2.3.

This hybrid model which incorporates elements of flamelet methods, and soot reaction modelling, is henceforth referred to as the *sootlet* model for the sake of brevity.

2.2.2 CMC-soot model

In contrast to the SLF method, the Conditional Moment Closure (CMC) method is not limited to modelling combustion phenomena which have length and time scales which are smaller than local mixing scales[1]. The ability of the CMC method to capture long timescale effects such as radiant heat loss and kinetically limited pollutant emission is well documented[13, 14, 15].

Using this method, the instantaneous equations for soot evolution are averaged conditionally upon mixture fraction,

$$\frac{\partial\langle Y_s \mid \eta\rangle}{\partial t} + \langle u_i \mid \eta\rangle\frac{\partial\langle Y_s \mid \eta\rangle}{\partial x_i} = \frac{1}{2}\langle\chi \mid \eta\rangle\frac{\partial^2\langle Y_s \mid \eta\rangle}{\partial\eta^2} + \langle\dot{w}_{s,Y} \mid \eta\rangle \ , \tag{22}$$

$$\frac{\partial\langle \Gamma_s \mid \eta\rangle}{\partial t} + \langle u_i \mid \eta\rangle\frac{\partial\langle \Gamma_s \mid \eta\rangle}{\partial x_i} = \frac{1}{2}\langle\chi \mid \eta\rangle\frac{\partial^2\langle \Gamma_s \mid \eta\rangle}{\partial\eta^2} + \langle\dot{w}_{s,\Gamma} \mid \eta\rangle \ . \tag{23}$$

In the above equations, $\langle \ldots \mid \eta\rangle$ denotes a term which has been averaged on the condition that the local mixture fraction ξ is equal to a value η; that is, only those values of the sampled scalar, where $\xi(\underline{x}, t) = \eta$ is simultaneously true, contribute to the average[1].

The conditional mean evolution equations (22) & (23) are solved concurrently with similar conditional mean equations for gas phase species, and *un*conditional mean equations for the first and second statistical moments of mixture fraction (ξ). The solution of the mixture fraction equations, and the assumption of an assumed form for the corresponding mixture fraction probability density function (PDF) allows the calculation of conditional mean scalar dissipation rate ($\langle\chi \mid \eta\rangle$) which is employed in equations (22) & (23). Conditional mean scalar dissipation rate is determined through the manipulation of,

$$\frac{\partial}{\partial t}(P_\eta) + \frac{\partial}{\partial x_i}(\langle u_i \mid \eta\rangle P_\eta) = -\frac{1}{2}\frac{\partial^2}{\partial\eta^2}(\langle\chi \mid \eta\rangle P_\eta) \ , \tag{24}$$

where the left hand side of the equation is known through the assumed form variations in the mixture fraction PDF, P_η. Variations in the assumed-form PDF are determined according to variations in computed mixture fraction mean and variance. The Beta function has many suitable features as an assumed form for mixture fraction PDFs [16], and was thus used for that purpose in this study. The conditional mean scalar dissipation rate ($\langle\chi \mid \eta\rangle$) is determined by integrating the left hand side of equation (24) twice with respect to mixture fraction between known boundary conditions [17], followed by division by the mixture fraction PDF profile.

The closure of the chemical source terms can be effected using a first order approximation in the conditional moments of the reacting species and temperature,

$$\langle\dot{w}_s(Y_s, \Gamma_s, T, \ldots) \mid \eta\rangle \approx \dot{w}_s(\langle Y_s \mid \eta\rangle, \langle\Gamma_s \mid \eta\rangle, \langle T \mid \eta\rangle, \ldots) \ . \tag{25}$$

Note that in contrast to the total inadequacy of the first order moment closure of equation (16), a first order conditional moment closure is usually sufficiently accurate for most species provided that the combustion system is not on the verge of extinction.

As mentioned above, the evolution of soot particles throughout a turbulent diffusion flame is closely linked to radiant heat transfer from the flame. As a consequence of this,

it is necessary to include the influence of energy loss through radiation in the conditional mean equation for standardized enthalpy (h_{st}).

$$\frac{\partial\langle h_{st} \mid \eta\rangle}{\partial t} + \langle u_i \mid \eta\rangle\frac{\partial\langle h_{st} \mid \eta\rangle}{\partial x_i} = \frac{1}{2}\langle\chi \mid \eta\rangle\frac{\partial^2\langle h_{st} \mid \eta\rangle}{\partial\eta^2} + \langle\dot{s}_h \mid \eta\rangle \ , \tag{26}$$

Earlier implementations of the CMC method have employed an optically thin radiation submodel [1, 13, 15] to determine the magnitude of the radiant source term ($\langle\dot{s}_h \mid \eta\rangle$). This model (see Section 2.3.2) is convenient in that it dispenses with the requirement for information concerning the local geometry of radiating elements with respect to one another, and so is easily implemented in a conditional averaged equation which may apply over a spatially distributed zone. The optically thin radiation submodel is applied in the CMC-soot model here where source term closure is first order in conditional mean temperature and soot mass fraction, as in the manner of equation (25).

Extensive discussion of the practical details of this model is provided elsewhere [1, 13]. The original descriptions of the CMC method also contain a wealth of useful information [18, 19]. As it stands the soot variant of the gas phase CMC model is little different in theoretical terms. A number of refinements may ultimately be necessary to improve the accuracy of the model.

One obvious improvement stems from the fact that the soot particles being modelled essentially do not diffuse at all compared to the surrounding gases. It is assumed that the particles are sufficiently small so that at high Reynolds number they are convected by small scale velocity fluctuations to the same degree as the surrounding gases. Even so, there will exist significant variations in local particle abundance and properties at scales below the smallest scales of motion where diffusion has 'smeared out' variations in the gas field. These local variations have the capacity to invalidate the first order conditional mean chemical closure described above, wherever the level of variation is large and/or the degree of reaction sensitivity is high.

Past research has been performed on the inclusion of second order conditional moment chemical closure [20, 21, 22] into the calculation of reactive scalars in turbulence. Li and Bilger [21] found that full second order chemical closure was essential and effective in predicting a single step isothermal reacting system in a turbulent scalar mixing layer. The simplicity afforded by the single step reaction in their case allowed a full second order closure (involving conditional *variances* as well as means of all reactive species) to be employed at little computational expense.

In multi-step chemical systems however, the cost of second order closure is much greater, and much less sure of success given the fact that many more conditional variance equations must be solved as well as (strictly speaking) conditional covariance equations between species. No clear methodology is apparent at this stage for how the variance and covariance equations themselves can be closed.

The assumed general importance of temperature over other reactive scalars in determining chemical reaction rates lead to the investigation of employing a closure that was second order in temperature only. Despite the direct numerical simulation findings of Smith [20] that show that partial second order closure (second order in temperature only) is generally not sufficient to improve closure for multi-step chemical reactions, Kronenburg

et al [22] have implemented such a scheme for predicting nitric oxide formation in hydrogen jet flames with simplified chemistry. Although inconclusive, their results indicate that a partial second order closure may be more effective than a simple first order closure alone. It may be possible to employ a partial second order closure in soot mass fraction and particle abundance in an effort to improve the closure of soot process rates.

The fundamental effectiveness of employing CMC modelling in the treatment of small reactive particles in turbulent combustion is currently the subject of analysis in a direct numerical simulation study [23].

2.3 Radiation modelling

A full and comprehensive treatment of radiant heat losses, involving say a Monte Carlo simulation, has not been incorporated into this study due to its associated computational overhead. In place of such a treatment, the following simplified models have been implemented. These models exploit the simplifications which result from assuming that the radiant environment *seen* by a radiating particle is either totally obstructed by surrounding particles, or totally unobstructed.

2.3.1 Optically-Thick Model

In the case of radiant heat transfer in the optically thick limit, radiation emitted by any given particle has an extremely short mean free path. Under these conditions, radiant heat transfer occurs between immediately adjacent particles only, with no transfer at all over extended distances. This approximation can reasonably be made in physically small combustion systems with high soot loads.

This type of radiant transfer of energy from the fluid is often referred to as the *diffusion approximation* [24] because of its mathematical similarity to heat and mass transfer through molecular diffusion. The rate of heat transfer from a single point at temperature T to its immediate surroundings, which are at an effective *radiant temperature* T_r, is given by,

$$\dot{Q} = 4\sigma K_a \left(T^4 - T_r^4\right) \tag{27}$$

where σ is the Stefan-Boltzman constant, and K_a is the local Rosseland mean absorption coefficient. In the diffusion limit, the local flux of energy in the *radiant background* is given by the following gradient expression.

$$q_i = -\frac{4\sigma}{3K_a}\frac{\partial}{\partial x_i}\left(T_r^4\right) \tag{28}$$

Combining the introduction of heat to the radiant background equation (27), and diffusional transport in the background , an equation describing heat transfer in the diffusion limit is derived,

$$\dot{Q} + \frac{\partial q_i}{\partial x_i} = 0 \ , \tag{29}$$

which can be written in terms of temperature as,

$$3K_a^2\left(T^4 - T_r^4\right) = \frac{\partial^2}{\partial x_i^2}\left(T_r^4\right) \ . \tag{30}$$

In practice a quantity representing the averaged fourth power of the radiant temperature ($\langle T_r^4 \rangle$) is solved for throughout the computational domain. The interaction of this field with the boundaries of the domain and with local fluid temperatures (T) through equation (27) acts as an energy transfer mechanism. Appropriate boundary conditions upon the above equation are discussed extensively by Siegel and Howell[24].

In order to solve for the radiant background field, information is required that pertains to the Rosseland mean absorption coefficient (K_a) in the presence of soot. This coefficient is simply an inverse spectral average of the Rosseland spectral extinction coefficients,

$$\frac{1}{K_a} = \int_\infty k_a^{-1}(\lambda) d\lambda \ . \tag{31}$$

The spectral extinction coefficient for soot in the Rayleigh limit, where the particles are small compared to the principal emitting wavelength, is given by the following expression provided by Lee and Tien[25],

$$k_a(\lambda) = \frac{36\pi n_r n_i}{(n_r^2 - n_i^2 + 2)^2 + 4n_r^2 n_i^2} \frac{f_{sv}}{\lambda} \ . \tag{32}$$

In the above expression, n_r and n_i represent the real and imaginary parts of the complex refractive index for soot, while f_{sv} is the soot volume fraction defined as,

$$f_{sv} = Y_s \rho / \rho_p \ . \tag{33}$$

It is clear from the equations above that radiant heat transfer in the optically thick limit involves the entire domain in the determination of radiation propagation to the boundaries. Energy can be transferred, for example, from a particularly hot portion of a flame to a nearby cooler zone, but only through an interaction with material in the intervening space. In reality, radiant heat transfer can frequently occur between hot and cold zones with minimal interaction with the intervening medium. The tendency towards interaction or non-interaction is governed by the absorptivity of the intervening medium.

2.3.2 Optically-Thin Model

The basis for an optically-thin radiation heat transfer approximation is that the media, between the initial point of emission and the domain boundary, does not participate in the transfer in any way. Under this assumption, radiant heat loss ($\dot{s}$) is solely a function of local conditions at the point of emission and temperature at the boundary (T_∞),

$$\dot{s} = 4\sigma K_p \left(T^4 - T_\infty^4 \right) \ , \tag{34}$$

where K_p is the Planck mean absorption coefficient.

The Planck mean absorption coefficient is determined as a simple average of spectral values,

$$K_p = \int_\infty k_{p,\lambda}(\lambda) d\lambda \ . \tag{35}$$

Values for the Planck mean absorption coefficients for Rayleigh-limit soot, molecular H_2O and CO_2, were determined using the RADCAL code of Grosshandler[26]. Temperature-dependent fifth-order logarithmic polynomial curve fits (p_s,p_{h2o},p_{co2}) were determined from

the RADCAL data for each species and was employed with soot volume fraction (f_{sv}) and gas phase partial pressures (ppH_2O,$ppCO_2$) in subsequent heat transfer calculations according to,

$$K_{p,s}(T, f_{sv}) = p_s(T) f_{sv} \ , \tag{36}$$

$$K_{p,h2o}(T, ppH_2O) = p_{h2o}(T) ppH_2O \ , \tag{37}$$

and

$$K_{p,co2}(T, ppCO_2) = p_{co2}(T) ppCO_2 \ . \tag{38}$$

The sum of the above three Planck mean absorption coefficients provides the overall Planck mean absorption coefficient for the local radiating environment.

The optically-thin radiation model has been employed successfully in the past for predicting heat transfer from turbulent non-sooting flames[1, 13, 15], and heat transfer from a laminar sooting flame[10]. The applicability of this model in the broader soot-rich 'brush' region of a sooting turbulent diffusion flame has not been established however. In all likelihood, the model is only applicable in certain zones of these flames, as is the optically-thick model described above. Both the optically-thick and optically-thin radiation models were tested in this investigation.

2.4 Numerical Implementation

The two modified turbulence-chemistry models (CMC-soot and *sootlet*) were implemented in connection with a commercially-available computational fluid dynamic (CFD) software package. This CFD package, known as TASCflow3D [27], allows flow and mixing fields to be solved in complex geometries such as those encountered in gas turbine combustors. Fortunately, TASCflow3D also provides substantial access via a source code interface (SCI) to allow for additional model implementation within the framework of the package.

As the TASCflow3D package already contained a steady laminar flamelet model for the prediction of nonpremixed gas-phase combustion, it was a relatively straightforward to incorporate the sootlet model along similar lines using SCI tools. In this way the sootlet model can be used by the TASCflow3D code during actual computation of combustion problems.

Unlike the sootlet model, it was found necessary to implement the CMC-soot model externally to the TASCflow3D package due to the significant computational overhead associated with its use. Typically, solution of the CMC-soot equations requires more memory and computation time than that required by a full standard TASCflow3D computation. The CMC-soot model was implemented so as to utilize a pre-computed flow field solution as input, and produce detailed thermochemical predictions as output.

The chemical mechanism used to describe the combustion of propane was that proposed by Leung *et al.* [28]. This mechanism consists of 31 reactive species and 111 individual reactions. The TASCflow3D package was used to solve for two dimensional axisymmetric flow and reaction on a multi-part grid comprising embedded refined subgrids with in excess of 65000 nodes. All computations made with TASCflow3D incorporated a sootlet model,

and took approximately 6-8 CPU hours and 156 Mb of memory to complete on a fast workstation.

Calculations made using the CMC-soot model involved the refinement of the initial TASCflow3D-sootlet results, and typically required 20-24 CPU hours and 91 Mb of memory to complete on a fast workstation.

References	[2, 6]
Nozzle Diameter (D) [mm]	2.00
Bulk Jet Velocity (U_j) [m/s]	30.
Cold Jet Reynolds Number	5,000
Convective Timescale (D/U_c) [s]	6.7e-5
Soot diagnostic techniques	physical

Table 2: Observed C_3H_8 flame conditions and characteristics

3 Results

Nishida and Mukohara [2] reported upon experimental observations of soot density and temperature in two different turbulent propane jet flames. and two transitional propane jet flames. Of the two turbulent flames, one burned in air preheated to five hundred degrees celsius, whilst the other had an air-stream temperature of only fifty degrees celsius (323 K). Model results for the latter flame were generated because the low level of preheat allowed flamelet libraries with 300 K air stream temperatures to be reasonably employed without having to enter into the lengthy procedure of generating further libraries. The primary descriptive features of the flame are given in Table 2.

3.1 Global flame characteristics

The inherent character of soot and temperature evolution in a sooting turbulent jet flame is illustrated in Figures 1 & 2. Predicted distributions of mean temperature, radiant power density (energy emission rate per unit volume), soot particle abundance (number of moles of particles per unit mass of mixture), and soot mass fraction (mass of soot per unit mass of mixture) are plotted from an axisymmetric jet flame calculation of the flame of Nishida and Mukohara. The jet flow direction in the figure is from bottom to top, with the fuel jet issuing from a two millimetre wide entry, centred on $y = 0$ at the bottom of the figure. The axial extent of the computational domain is greater than six hundred nozzle (Figs 1 & 2 are confined to the first 300 diameters) inner diameters in length, while the stoichiometric length of the flame is predicted to be approximately 260 diameters.

The qualitative influence of soot particle formation and agglomeration (as represented by the modelled processes) can be inferred from the right hand plot of Fig. 1. It is evident that the number of soot particles is greatest at around one quarter of the stoichimetric flamelength and that the particles are closely confined to a narrow range of hot but relatively fuel rich gas. Thereafter, the abundance of particles drops gradually as the particles agglomerate. The presence of large amounts of soot precursors at high temperatures upstream of the stoichiometric flametip facilitates the increase in particle numbers in spite of concurrent agglomeration. It is the absence of these soot precursors in the regions of the flame downstream of the flametip which allow agglomeration to shift the balance in favour of a reduction in particle numbers.

The total mass of carbon bound up as soot in the flame is distributed in a more concentrated pattern than that for the number of soot particles. The processes of surface

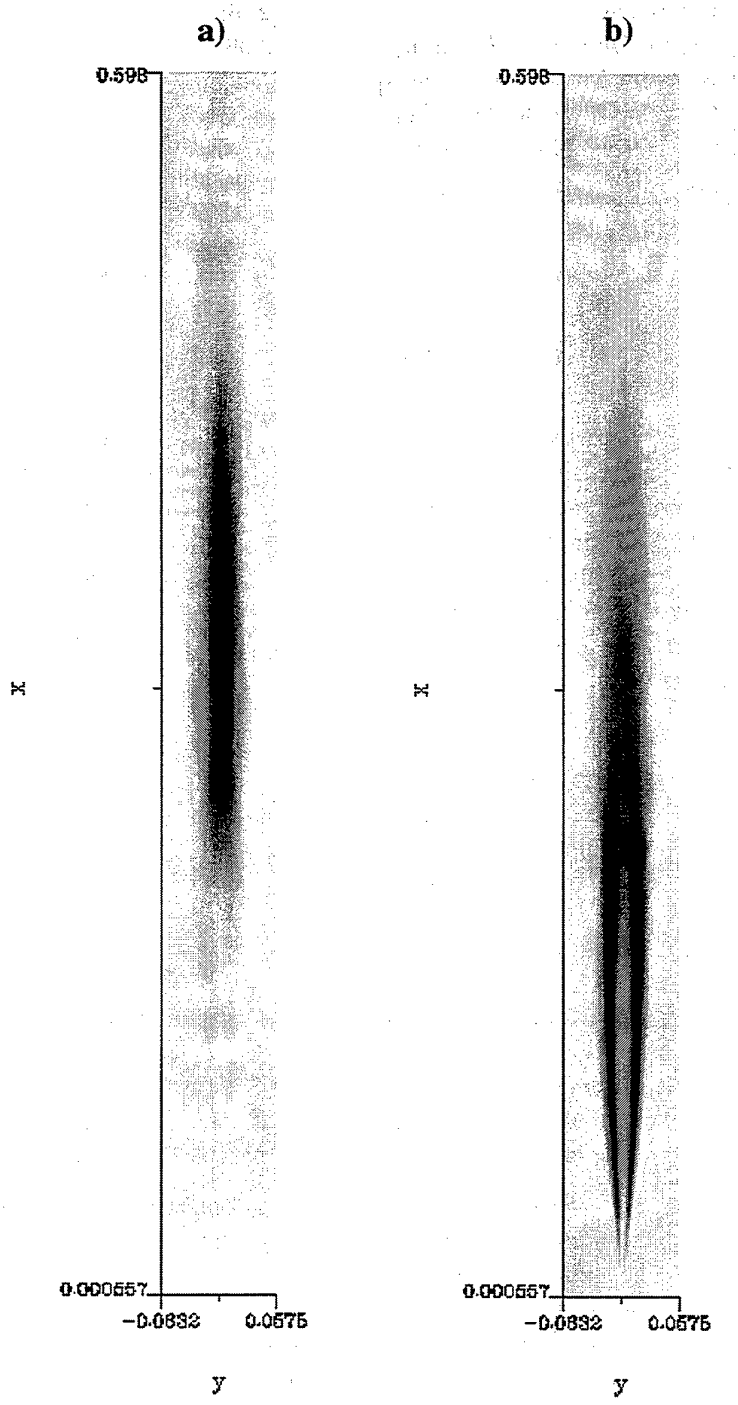

Figure 1: Qualitative form of predicted mean soot mass fraction (left) and soot particle abundance (right) distributions for an axisymmetric jet flame.

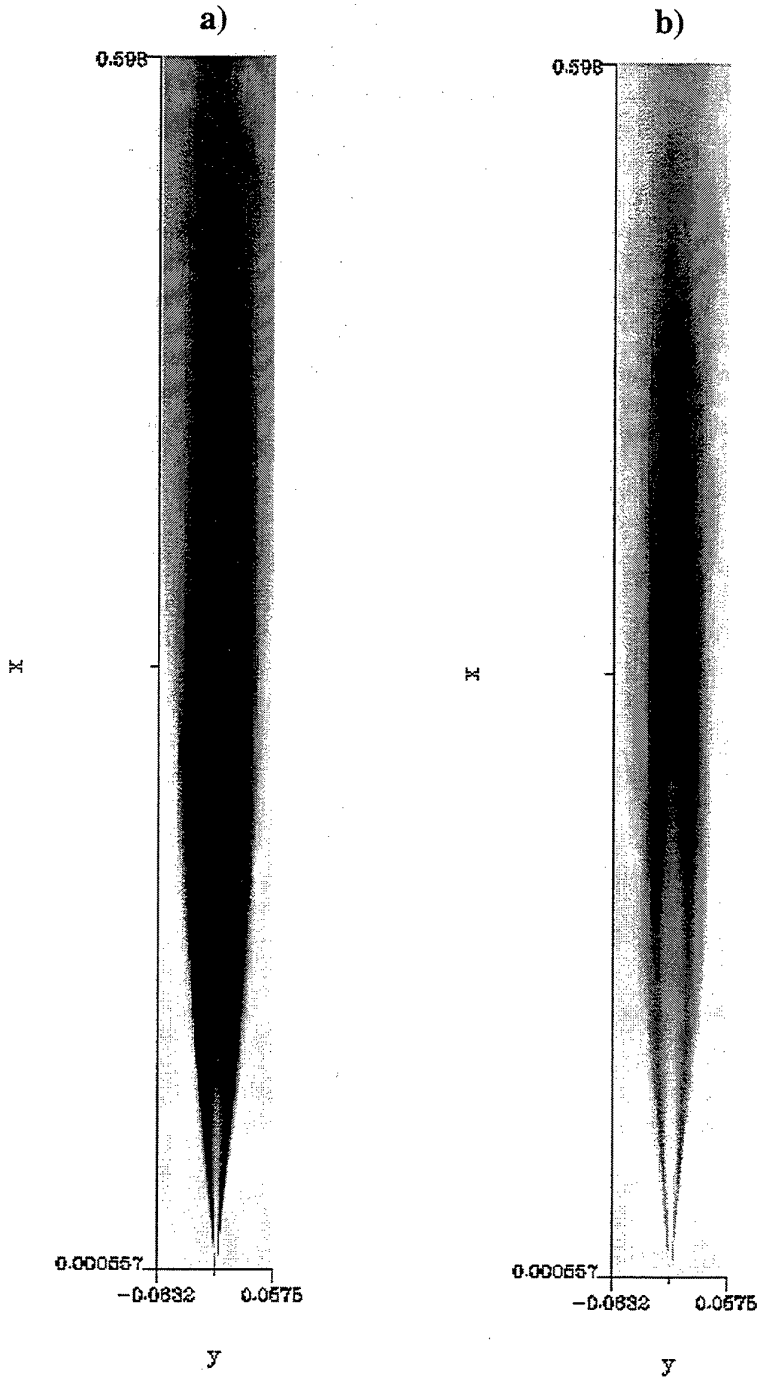

Figure 2: Qualitative form of predicted mean temperature (left) and radiant power density (right) distributions for an axisymmetric jet flame.

growth and oxidation are closely balanced in their action upon established soot particles. The peak soot density occurs on the centreline at a location that is significantly upstream from the stoichiometric flametip. Soot mass rises sharply on the jet centreline, increasing through many orders of magnitude in a short distance as a result of the positive feedback effect of surface area upon surface area growth. The zone of peak soot density also corresponds with a region of relatively cool gas (see Fig. 2) , largely as a consequence of radiant heat losses from soot in this region. The absence of large amounts of soot mass in the outer hotter regions of the flame upstream of the flametip is a result of the strong oxiding environment that is found there. The steady decline in the concentrations of the gaseous precursors necessary for soot surface growth leads to a decline in surface growth nearer to the flametip. This trend in concert with the direct oxidation of the soot particles results in a rapid decline in soot mass towards the flametip and thereafter.

Beyond the flametip, agglomeration and oxidation of soot continues, but at a reduced rate owing to the progressively lower gas temperatures and progressively more dilute soot particle abundances. The mass of soot which escapes the flame envelope on the centreline is approximately an order of magnitude lower than the peak centreline value. As smoke, the escaped soot particles become inert as they cool when mixed with further entrained air.

The temperature distribution plotted in the left hand side of Fig. 2 is reminiscent of all nonpremixed jet flames in that the zones of highest temperature correspond closely with the regions where fuel and oxidizer have been mixed to stoichiometric proportions. These stoichiometric zones envelope the fuel jet from the nozzle exit plane out to the stoichiometric flametip. The presence of radiant heat loss from the flame is also in evidence, however. The peak temperature in the distribution occurs not on the centreline near the flame tip, as one might except in an adiabatic flame, but on the mean stoichiometric contour at an upstream location off the centreline. The effect of radiant losses is to cause the flametip to be noticeably cooler than upstream stoichiometric zones despite its relatively quiescent mixing state. The right hand plot of Fig. 2 indicates that the region of peak radiant energy emission coincides with the region of peak soot mass. The high levels of soot present give rise to a high degree of heat transfer from the flame somewhat upstream from the flametip.

It will be seen in the following that the treatment of radiation losses and their effect upon flame temperatures plays a crucial role in the effectiveness of the soot models described above.

3.2 Sootlet model predictions

As discussed in Section 2.1, the rate coefficients for the Arrhenius steps of soot evolution were largely determined by Leung *et al* [5] and Fairweather *et al* [6] to be those which gave best agreement between soot formation predictions and available experimental data. In so doing, however, the treatment of other non-chemical processes such as radiant heat loss must have had a bearing on the resultant coefficients. Indeed there is disagreement between the value of the coefficients between the two sources [5, 6] according to the type of flow case studied, with the former applying for laminar flames, and the latter for turbulent flames.

Case No.	Radiation factor	Growth factor	Oxidation factor	$x_{\hat{T}_c}[m]$	$x_{\hat{Y}_c}[m]$	$\hat{T}_c[K]$	$\hat{Y}_c$
Expt.	n.a	n.a	n.a	0.45	0.35	1590	2.0e-3
s2	1.0	0.20	0.20	0.38	0.35	1807	6.35e-3
s3	1.0	0.10	0.20	0.45	0.34	1956	2.40e-3
s4	2.0	0.10	0.20	0.44	0.34	1876	2.24e-3
s5	2.0	0.20	0.20	0.30	0.34	1723	5.21e-3
xs1	1.0	0.15	0.20	0.43	0.36	1879	4.1e-3
xs2	1.0	0.20	0.15	0.38	0.37	1826	5.8e-3
xs3	1.0	0.25	0.20	0.34	0.37	1775	8.0e-3
xs4	1.0	0.50	1.00	0.53	0.33	1742	1.2e-2
xs5	2.0	1.00	1.00	0.21	0.31	1564	1.7e-2
xs6	2.0	0.50	1.00	0.25	0.32	1640	9.7e-3
xs7	2.0	0.25	1.00	0.50	0.30	1883	4.3e-3
xs8	2.0	0.10	2.00	0.45	0.29	2014	6.7e-4
xs9	2.0	0.20	2.00	0.46	0.29	1990	2.2e-3
xs10	4.0	1.00	1.00	0.19	0.30	1521	1.2e-2
xs11	4.0	0.50	1.00	0.22	0.32	1590	7.1e-3
xs12	1.0	0.15	0.20	0.41	0.36	1819	3.17e-3

Table 3: Summary of flame characteristics predicted by sootlet model with variations in governing parameters in soot rates and radiant heat loss. Note that all cases, save the last, were calculated using an optically thick radiation model. The last case was calculated using an optically thin model.

Owing to the implementation of a more realistic treatment of radiant heat loss in this study (see Section 2.2.1), and the allowance for the effect of local straining upon C_2H_2 levels, some modification of the rate coefficients used by Fairweather *et al* was warranted. A limited parametric study of the effects of varying the rate coefficients for soot surface growth and oxidation was performed. Modfication to radiant heat losses was incorporated through a parametric adjustment factor. The adjustment factor was used to gain some indication of what effect changes in the magnitude of heat loss can have on the distributions of soot and temperature.

Temperature and soot characteristics of the cases trialled in the parametric study of the sootlet model prediction of the Nishida-Mukohara flame are provided in Table 3 as entries *s2* through *s5*. Among the tabulated characteristics, are the axial locations where maximum centreline soot mass fraction and temperature occur ($x_{\hat{T}_c}, x_{\hat{Y}_c}$), and the corresponding values at those locations ($\hat{T}_c, \hat{Y}_c$). The factors given for growth and oxidation were the real constants by which the pre-exponential rate coefficients in Table 1 were multiplied. The radiation factor was the applied everywhere to the Rosseland mean extinction coefficient in the case of the optically thick radiation model (see Section 2.3.1), and the Planck mean absorption coefficient in the case of the optically thin model (see Section 2.3.2), which was applied in *xs12* only.

The additional entries, *xs1* through *xs12*, in Table 3 correspond to the same jet flame but without the radial confinement present in the experimentally observed flame. This latter group of predictions were found to provide a useful guide as to the effect of varying the studied parameters, but were not comparable to the experimental profiles due to the difference in the degree of confinement.

Representative predictions within the parametric range are compared with experimental measurements of axial variation in centreline mean temperature and normalised soot density in Figs 3 & 4. Normalised soot density is defined as the mass of soot per unit volume of mixture, where the gas mixture has been returned to a standard temperature (300 K). Computation of normalised soot density was made by post-processing soot mass fraction data simultaneously with mean temperature and density while assuming frozen chemical composition between the *in situ* and cooled sample states. The use of soot density as a comparative variable is an artifact of the soot collection techniques employed by Nishida and Mukohara [2].

It is clear from Fig. 3 that it was not possible to find good qualitative and quantitative profile agreement between any given predicted profile and the measured profile. In general it was found that those profiles whose input parameters gave rise to good agreement in the vicinity of the soot density peak, tended to grossly overpredict the rate of soot destruction beyond the peak. Those profiles with rates of soot destruction downstream of the peak, similar to the experimental rates, had peak values far in excess of the experimental profile.

The predicted profiles, as a group, differ from the experimental profile in the extreme upstream portion of the flame. It is apparent that the experimental soot density profile has values that exceed the predicted profile values by around one thousand percent. Clearly, the current model for soot formation does not account for the substantial level of soot density on the centreline at the extreme upstream range of the measured data. This may be due to unaccounted complexities in the particle nucleation process. In the same vicinity, the axial rate of growth of soot density on the centreline is predicted by all cases to be

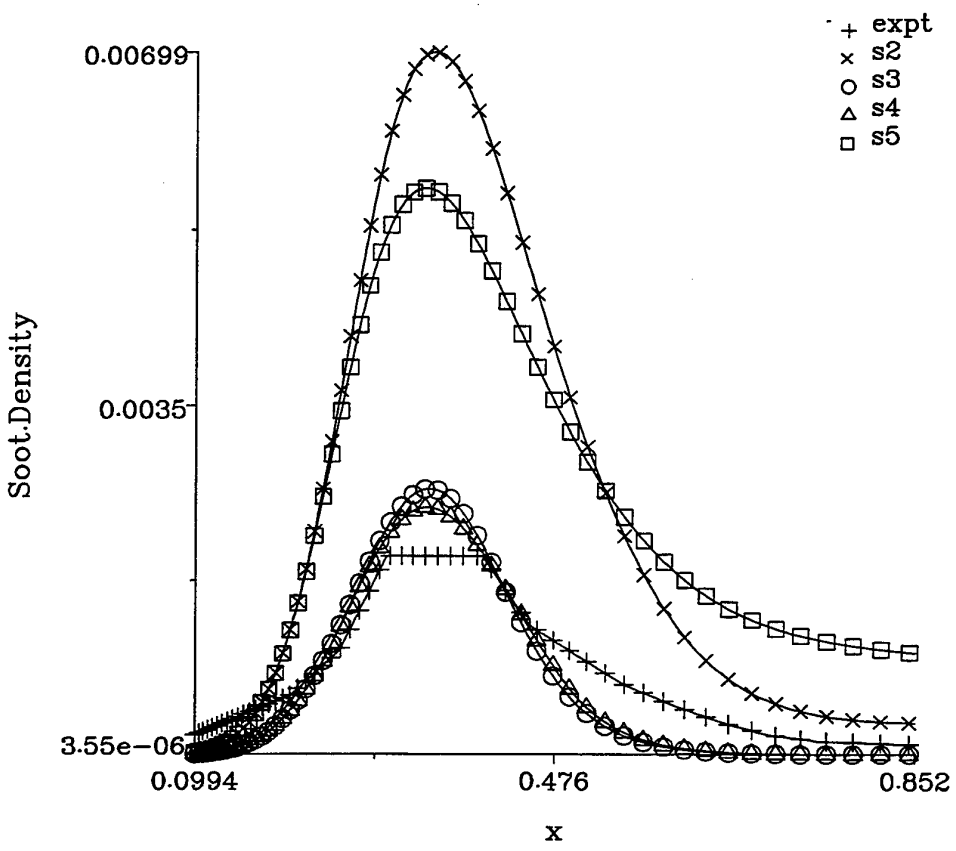

Figure 3: Mean normalised soot density profiles (in kg / cubic m) from experiment and sootlet *model predictions for the jet centreline. Legend designations correspond with entries in Table 3*

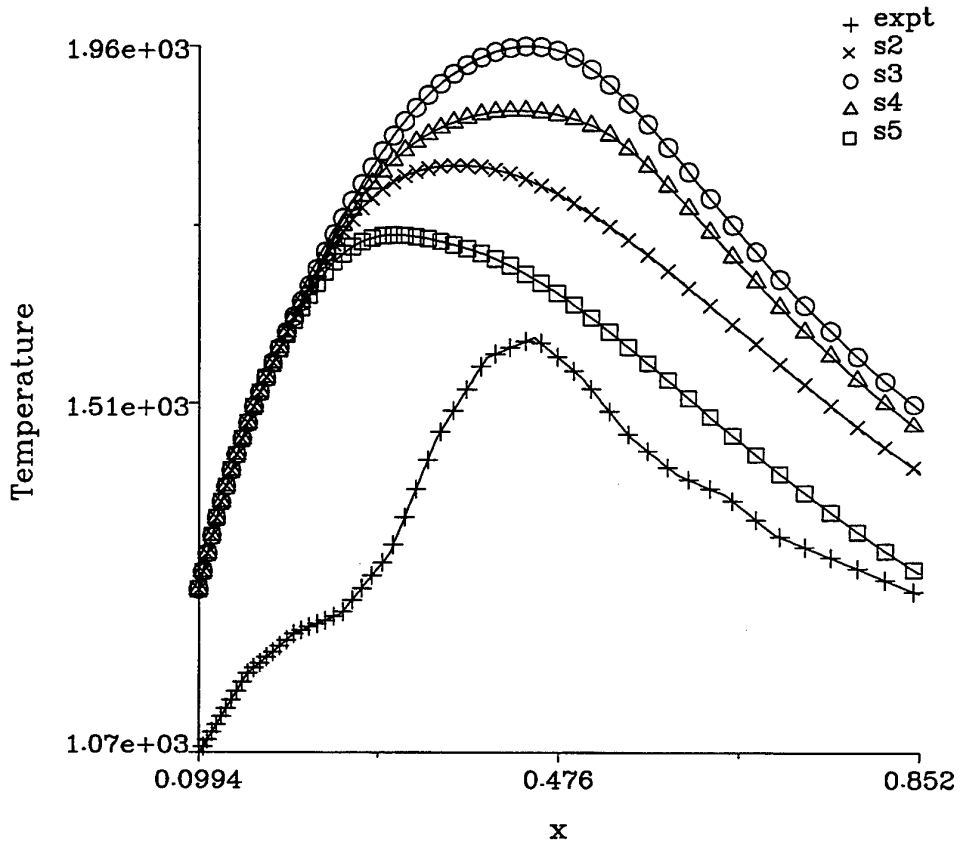

Figure 4: Mean temperature profiles (in degrees K) from experiment and sootlet model *predictions for the jet centreline. Legend designations correspond with entries in Table 3*

significantly greater than that which was observed experimentally. This higher rate of growth can be explained with reference to the comparison of temperature profiles.

From Fig. 4, it can be seen that the predicted temperature profiles collapse onto a single curve out to an axial distance of about ($x = 0.22$, $x/D = 109$). This curve lies more than two hundred and fifty degrees Kelvin above the experimentally measured temperature profile. Beyond $x/D = 109$, the predicted temperature profiles rapidly diverge according to variations soot surface growth and its effect upon radiant heat loss, and the value of the radiation adjustment factor (see Table 3). The fact that the profiles are coincident upstream of this location suggests that the influence of radiation in these zones is predicted to be slight. This may be a result, at least in part, of the much lower levels of soot predicted for these zones of the flame, compared to what was observed experimentally.

The range of conditions studied allows some general trends to be observed for soot formation with variation in the soot rates and the artificially modified radiant heat loss. For instance, refering to Fig. 3, notice the differences between the profiles for cases *s2* and *s3*, and *s4* and *s5* (see Table 3). In each comparison, the parametric variation in the soot surface growth rate results in an approximately proportional increase in the value of the peak soot density, while the location of peak density is seemingly unchanged. A comparison of cases with equal soot surface growth rates but different radiation adjustment factors (eg. cases *s2* and *s5*, and *s3* and *s4*), indicates that the higher growth cases show a much more marked divergence from one another, particularly in the downstream zones of the flame.

Refering to Fig. 4, it can be seen how the above behaviour can largely be attributed to differences in local mean temperatures. The mean temperature profiles of the high soot growth rate cases (*s2* and *s5*) are depressed by hundreds of degrees below the profiles corresponding to lower soot growth. The peak mean temperature on the centreline in the high soot cases occurs much closer to the nozzle than in the low soot cases and has a lower value. The high levels of soot which form in cases *s2* and *s5* are accompanied by a high level of radiant heat loss from the flame centreline. This is particularly true for the high soot growth case where the radiation adjustment factor is doubled (*s5*). This depression of the local mean temperatures in the downstream portion of the flame retards the processes of soot oxidation on the centreline, with the result that the coolest flame in the parametric study emits the greatest soot.

In general, the predicted temperature profiles lie above that reported by Nishida and Mukohara [2]. There is a tendency for too rapid rates of soot surface growth and oxidation to be predicted as a result. This behaviour is likely due to a short-coming of the radiation model employed, and is discussed further in connection with its impact on soot predictions in Section 4.

3.3 CMC-soot model predictions

The study of CMC-soot model predictions for the flame of Nishida and Mukohara [2] was also conducted along the lines of parametric variation in the soot rate coefficients for surface growth and oxidation, as well as arbitrary modification (by multiplication by a constant) of the radiant losses predicted from an optically thin radiation model. Note that

Case No.	Radiation factor	Growth factor	Oxidation factor	$x_{\hat{T}_c}[m]$	$x_{\hat{Y}_c}[m]$	$\hat{T}_c[K]$	$\hat{Y}_c$
Expt.	n.a	n.a	n.a	0.45	0.35	1590	2.0e-3
c3	1.0	0.50	14.0	0.29	0.28	1573	2.81e-3
c4	1.0	0.20	14.0	0.32	0.30	1610	9.91e-4
c5	0.5	0.20	14.0	0.37	0.32	1786	2.01e-3
c6	1.0	0.20	1.00	0.31	0.31	1595	1.38e-3
c7	0.5	0.50	14.0	0.35	0.29	1736	4.78e-3
xc1	1.0	1.00	1.00	0.24	0.26	1518	6.2e-3
xc2	1.0	1.00	2.00	0.24	0.26	1528	5.8e-3
xc3	1.0	1.00	8.00	0.25	0.26	1543	5.3e-3
xc4	1.0	1.00	14.0	0.25	0.26	1547	5.2e-3
xc5	1.0	0.50	14.0	0.29	0.28	1587	3.0e-3
xc6	1.0	0.10	14.0	0.33	0.31	1637	3.9e-3
xc7	1.0	0.05	14.0	0.34	0.31	1642	1.3e-4
xc8	0.5	0.10	14.0	0.39	0.34	1808	8.3e-4
xc9	0.5	0.20	14.0	0.39	0.33	1794	2.1e-3
xc10	0.25	0.10	14.0	0.43	0.30	1934	1.0e-3

Table 4: Summary of flame characteristics predicted by CMC-soot model with variations in governing parameters in soot rates and radiant heat loss. Note that all cases employed an optically thin radiation model.

in contrast to the optically thin model application in the sootlet model (see Section 3.2), radiant losses were determined using the approximation of the fourth power of conditional mean temperature ($\langle T \mid \eta \rangle^4$). This approximation is vastly better than the approximation (to the mean fourth power of temperature) employed above and does not suffer from the same problem of heat loss underprediction.

In general, the level of heat loss from the CMC-soot predicted flames is substantially greater than in the case of the sootlet model predictions. This fact can be attributed to the use of an optically thin radiation model, which tends to overpredict heat losses at all locations. It is for this reason, that the parametric study of CMC-soot predictions (see Table 4) involved a parametric decrease in radiant heat loss over actual level, instead of the parametric increase employed in the study of Section 3.2. As with, the cases described in previous section, those in Table 4 denoted as *xc1* through *xc10* refer to an unconfined jet flame which cannot be directly compared with the experimental data.

Selected cases from the parametric range tabulated in Table 4 are plotted in terms of unconditional mean centreline soot density (see Section 3.2 for definition) and temperature in Figures 5 & 6.

Through careful, though wholly arbitrary, variations in soot rates and radiation losses, it was found to be possible to achieve marginal qualitative and quantitative soot density profile agreement between experiment and prediction. The same cannot be said for agreement between temperature profiles, where, though markedly improved in magnitude compared with the sootlet predictions, the qualitative agreement with experiment was poor.

The inclusion of an adiabatic equilibrium (or *fast chemistry*) flame prediction to the profiles of Fig. 6 was done to illustrate the effect of restricted air volume in the case of the experimental flame. Notice that the rate of decrease in centreline mean temperature in the case of the adiabatic equilibrium prediction is much the same as the experimentally observed case. Since the adiabatic prediction is free from all radiation heat losses, only cooling through the admixture of surrounding air can contribute to the decay in centreline temperature beyond the flametip. The similar decay rate of the observed profile can be taken as an indication that the degree of radiant heat loss from the experimental flame is quite modest in the downstream zones. This is particularly true in comparison with the radiating predictions which show a markedly steeper rate of centreline temperature decay in these zones.

The predicted temperature profiles all exceed the experimental profile by around one hundred and fifty degrees at the upstream measurement point. This discrepancy is similar to that found from analysis of the *sootlet* model predictions in the preceding section. As with the sootlet model predictions, it is plausible that the predicted absence of appreciable levels of soot upstream of the first measurement point may be a contributing factor. The overprediction in temperature in these zones is a strong influence over why the predicted upstream axial growth of soot is greater in all cases than what was observed experimentally.

Comparison of the predicted mean soot-density profiles corresponding to cases *c6* and *c4* (see Table 4) reveal the effect of varying the rate of soot oxidation while keeping all other parameters constant. In the latter case, a fourteen-fold increase in soot oxidation rate was chosen due to its earlier use by Fairweather *et al* [6] and Kennedy *et al* [10] in the prediction of sooting flames. It is evident that the higher oxidation rate case has improved agreement with the experimental soot density profile towards the end of the flame, however agreement is still too poor to produce a reliable estimate of, say, overall smoke emission. The influence of the predicted flame temperature in these two cases is pronounced. Both cases *c6* and *c4* (only c4 is plotted) can be characterised as dramatically underpredicting centreline mean temperature from about two thirds of the flamelength onwards. The low values of predicted temperature greatly inhibit what should be a fairly vigorous rate of destruction of soot. It is a tendency of the optically thin radiation model to overpredict heat loss, which has led to their particularly depressed temperature profiles in cases *c3*, *c4* and *c6*.

The influence of varying the soot surface growth rate can be seen by comparing the profiles of cases *c3* with *c4*, and *c5* with *c7*. The two hundred and fifty percent increase in soot surface growth rate between cases *c4* and *c3* corresponds to a 284 % increase in the peak centreline soot density. The increase in growth rate also tended to shift the location of the peak towards the nozzle slightly. The same change in soot growth rate going from case *c5* to *c7*, at a lower rate of radiant heat loss, gave rise to a 237 % increase in the peak soot density and another shift in peak location towards the nozzle.

Cases *c5* and *c7* are the result of an attempt to curb the excessive temperature depression seen for earlier cases, through the arbitrary halving of the radiant heat loss predicted by the optically thin radiation model. From Fig. 5, it can be seen that this reduction in heat loss gave rise to a 202 % increase in the peak soot density for the low soot growth cases (*c4* and *c5*), and a 170 % increase for the high soot growth cases (*c3* and *c7*). Decreased radiation loss tended to shift the location of the peak soot density away from the

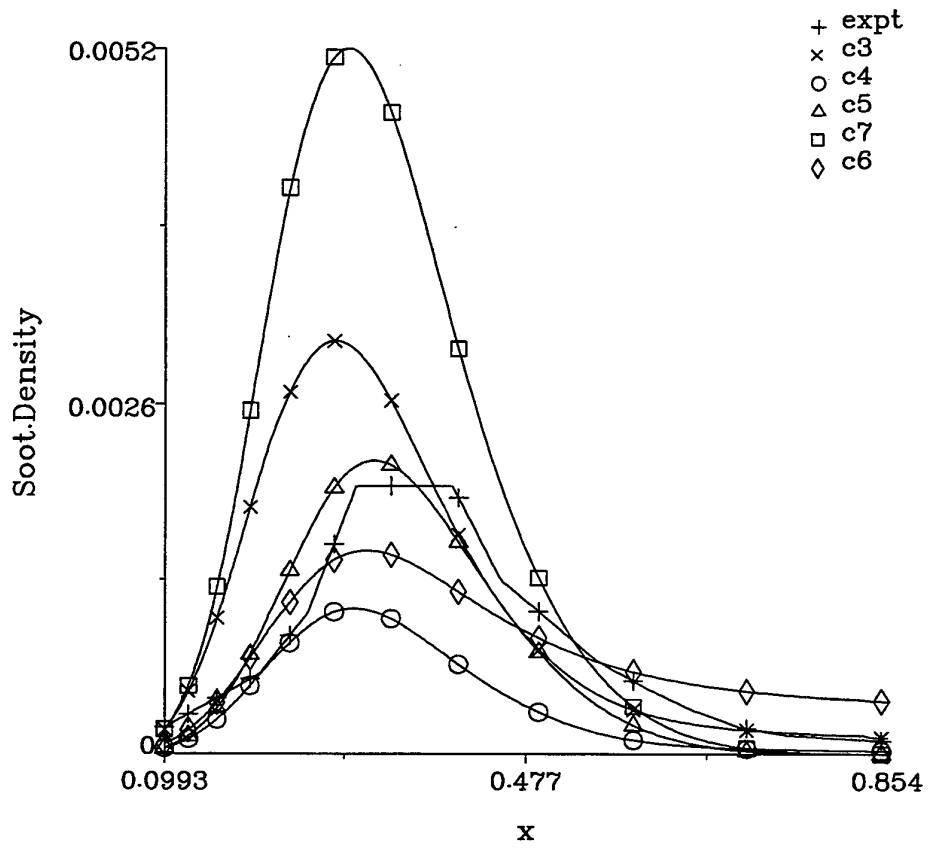

Figure 5: Mean normalised soot density profiles (in kg / cubic m) from experiment and CMC-soot *model predictions for the jet centreline. Legend designations correspond with entries in Table 4*

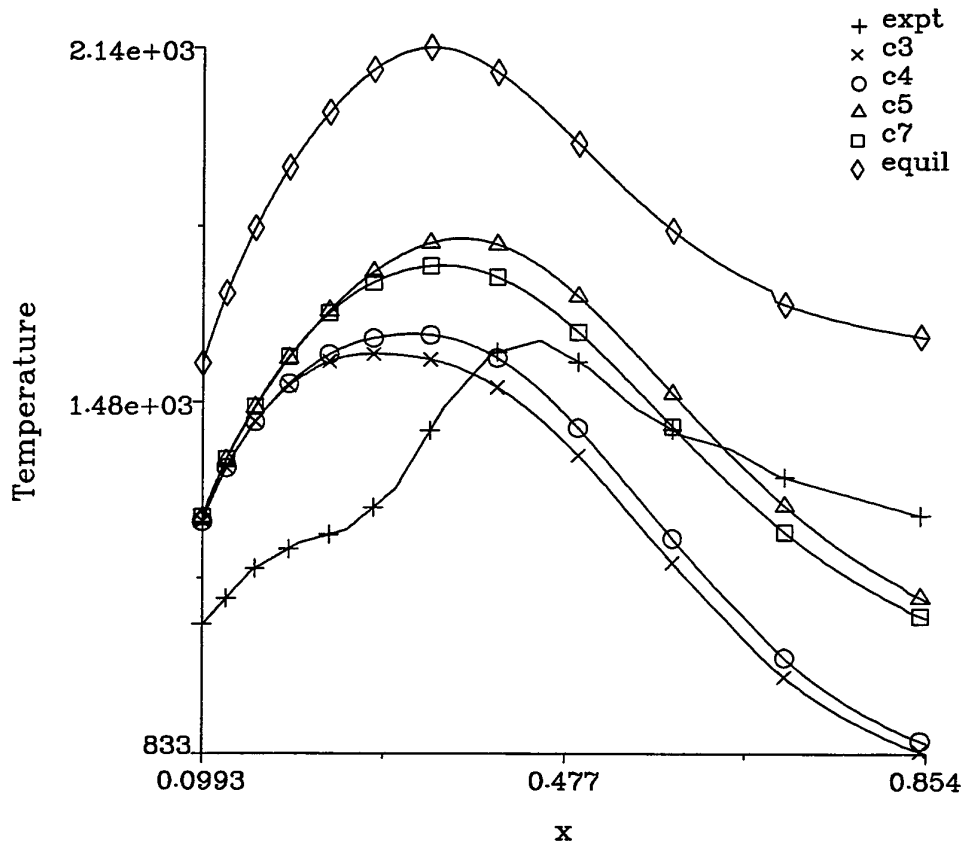

Figure 6: Mean temperature profiles (in degrees K) from experiment and CMC-soot model *predictions for the jet centreline. Legend designations correspond with entries in Table 4, except* equil *which denotes adiabatic chemical equilibrium.*

nozzle in each pair of cases.

It can be seen from Fig. 6, that the predicted temperature profiles corresponding to case pairs with similar radiation adjustment factors agree closely, despite a significant difference in the predicted soot densities (owing to differing soot surface growth rates). This agreement between the paired temperature profiles can be interpreted as being the result of the relatively small contribution made by soot at these levels to radiant heat loss compared to the contribution made by the molecular species, CO_2 and H_2O (see section 2.3.2). The emission of radiation by the molecular species is not a function of the local soot levels.

The predicted temperature profiles corresponding to the reduced radiation adjustment factor do not agree with the measured profile to any greater extent than the unmodified profiles. This indicates that the arbitrary halving of the radiant losses predicted by the optically thin model is not, as you would expect, an appropriate treatment to improve predictions of heat transfer from the flame. It is clear that the optically thin model does not provide a good description of the heat loss from a sooting flame either qualitatively or quantitatively. This issue is discussed in more detail in Section 4.

3.4 Conditional mean data predictions

Conditional mean data profiles provide an insight into the local thermochemistry which occurs in nonpremixed turbulent combustion. Unfortunately, conditional mean data was not contained in the Nishida and Mukohara paper [2], however it is nonetheless instructive to analyze the model results from the parametric study.

Conventionally (Favre) averaged data are determined from the conditionally averaged data through convolution with the local mixture fraction probability density function. For this reason, not all portions of a conditional mean profile contribute equally to a local *un*conditional average. Figure 7 is a plot of the logarithim of the cross-stream integrated density weighted mixture fraction PDF for various axial locations in the CMC-soot case *c7*. The relative weight accorded the different zones of mixture fraction space is proportional to the value of the PDF in that zone. It can be seen that as the jet fluid mixes with surrounding air, the mixture fractions which have the highest weight are at leaner and leaner values up until about $x/D = 225$ whereupon untainted air is no longer present. Thereafter, the PDF tends to have peak value at a mixture fraction which corresponds to the overall mixture fraction of the flow in the combustor. The significance of rich mixture fraction conditional mean data is greatly reduced towards the end of the flame. In the following data presented, the richest value of mixture fraction shown in each plot corresponds with the onset of the region of marginal probability.

In the CMC-soot method, conditional mean data is employed by the model for all species, in this case, thirty-four in all. In this discussion, we restrict our attention to three pertinent species. Figures 8, 9 & 10 contain plots of conditionally averaged data for soot mass fraction, soot particle molar abundance, and temperature. Each figure consists of plots for the various cases given in Table 4 at axial locations of $x = 0.15m$ $(x/D = 75)$, $x = 0.3m$ $(x/D = 150)$, $x = 0.45m$ $(x/D = 225)$, and $x = 0.6m$ $(x/D = 300)$. Each of the profiles is assumed to apply equally across the entire radius of the flame at each

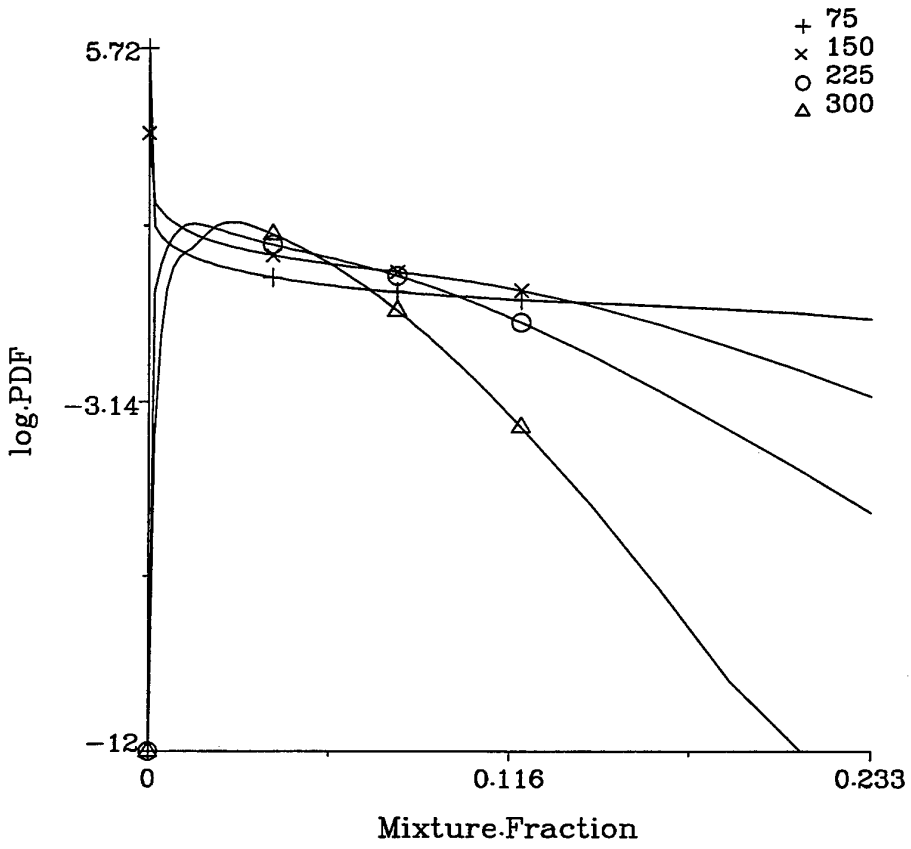

Figure 7: Logarithm of the cross-flame integrated density weighted mixture fraction probability density function from CMC-soot model predictions (case c7) at various axial locations. Legend designations correspond to axial location in nozzle diameters.

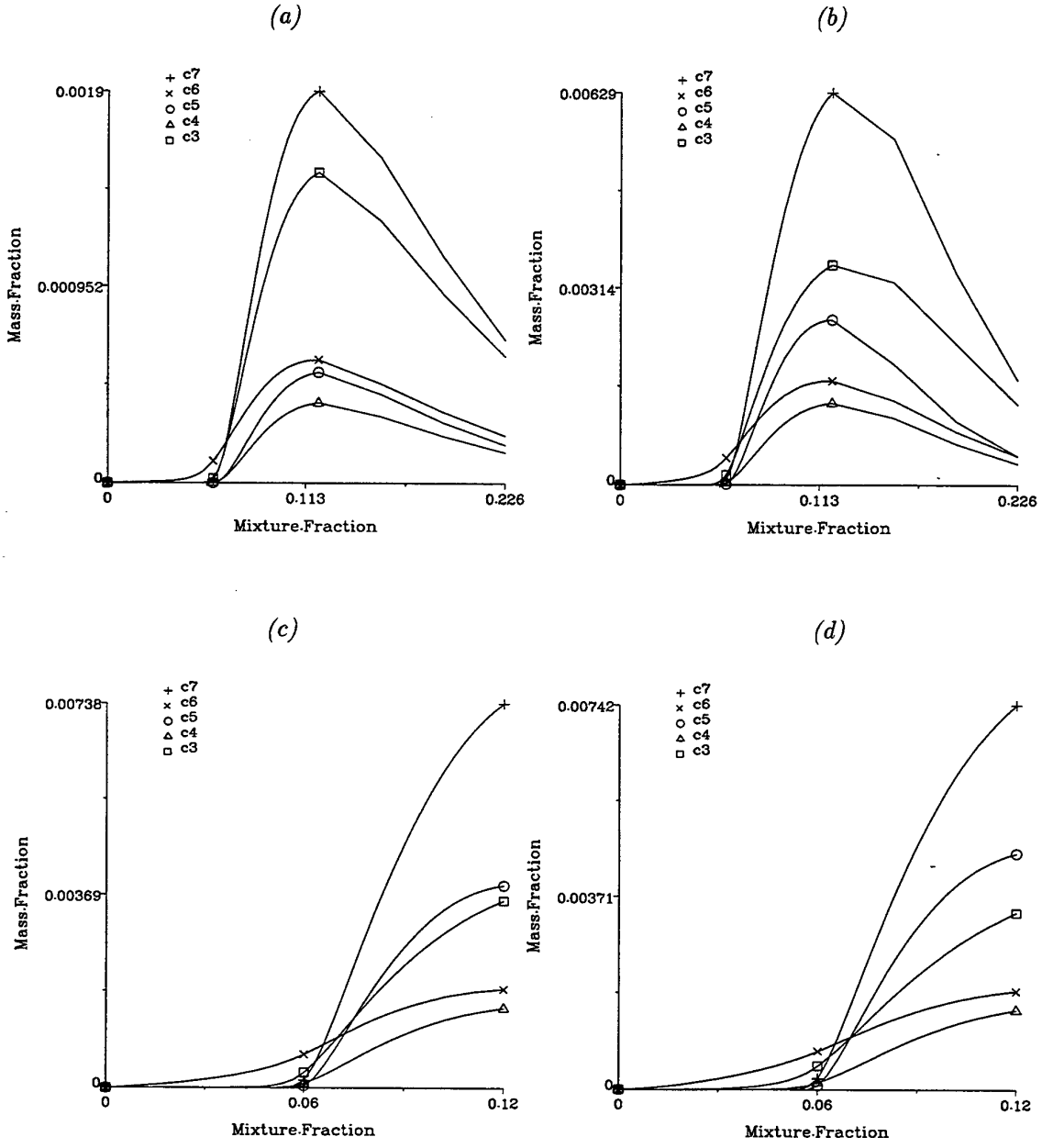

Figure 8: Conditional mean soot mass fraction profiles from CMC-soot model *predictions. The figure panels correspond to axial locations: a) $x = 0.15$, b) $x = 0.3$, c) $x = 0.45$ and d) $x = 0.6$. Legend designations correspond with entries in Table 4.*

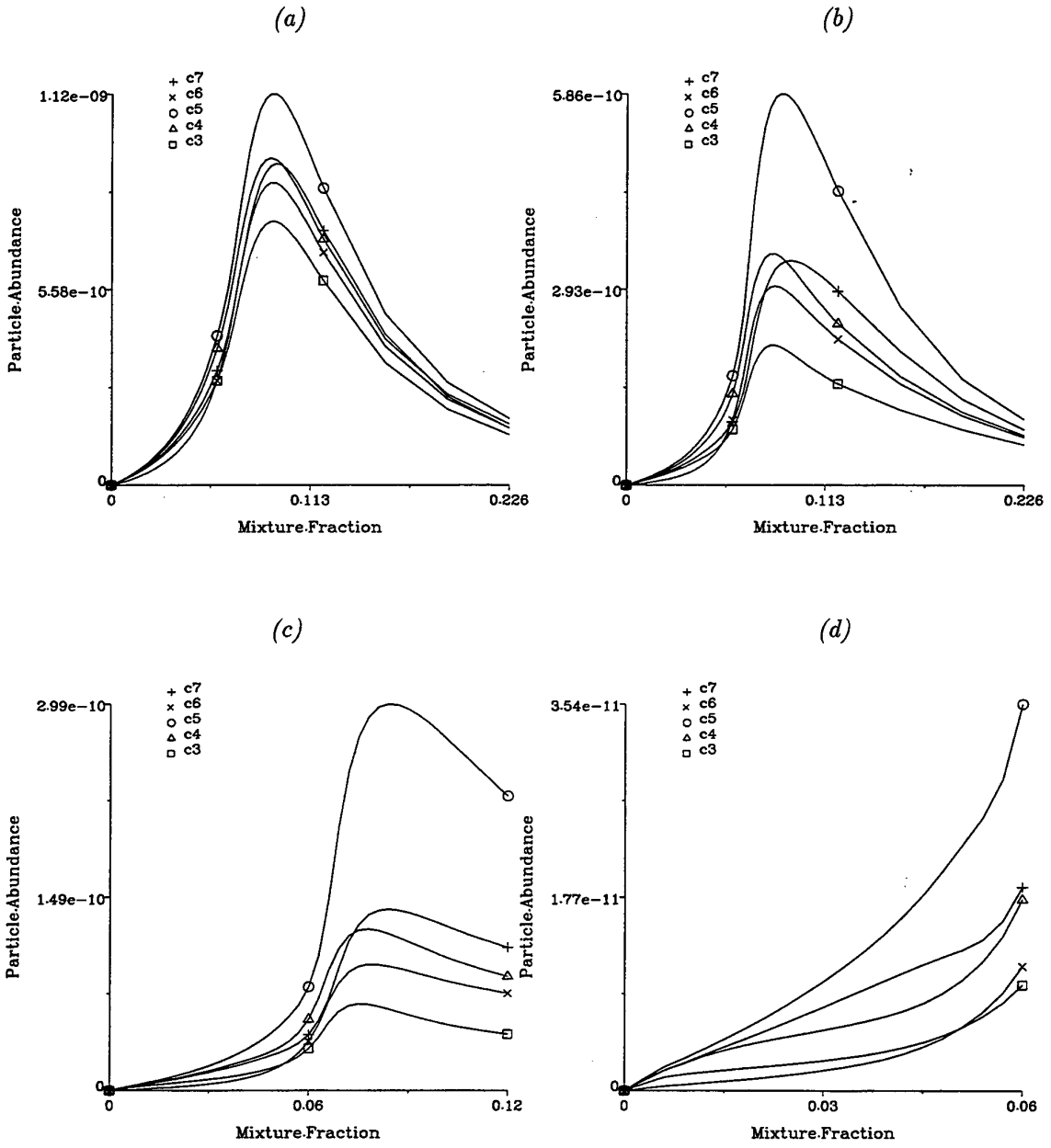

Figure 9: Conditional mean soot particle molar abundance (in moles per kilogram of mixture) from CMC-soot model *predictions. The figure panels correspond to axial locations: a) $x = 0.15$, b) $x = 0.3$, c) $x = 0.45$ and d) $x = 0.6$. Legend designations correspond with entries in Table 4.*

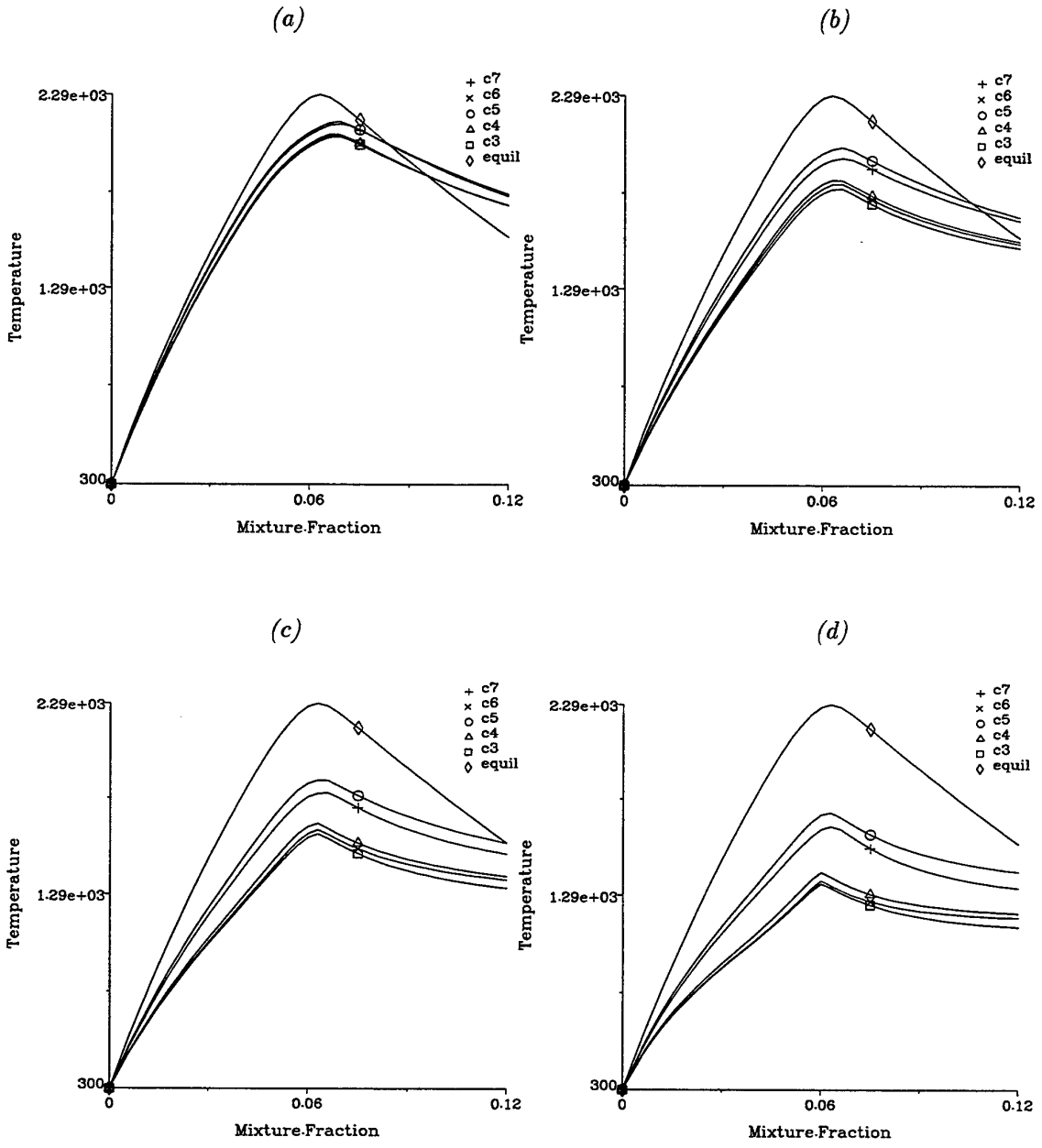

Figure 10: Conditional mean temperature profiles (in degrees K) from CMC-soot model *predictions. The figure panels correspond to axial locations: a) $x = 0.15$, b) $x = 0.3$, c) $x = 0.45$ and d) $x = 0.6$. Legend designations correspond with entries in Table 4.*

axial location. Justification for this assumption has been found both theoretically [17] and experimentally [29] in the past.

In Fig. 8, it can be seen that the vast bulk of soot mass is formed at rich mixture fractions in the vicinity of double the stoichiometric mixture fraction ($\xi_{stoic} = 0.06$). Mixtures of this composition, have both high levels of hydrocarbon intermediates which lead to soot (C_2H_2 in the case of the model), and a relatively high temperature. It is apparent from the steep gradients in soot mass fraction in mixture fraction space near stoichiometric that soot mass is being consumed through surface oxidation. It is also clear that no consumption of soot mass occurs on the rich side of the peak mass fraction zone, but that soot is transported from the formation zone to richer compositions through mixing action. The apparent shift in the centreline unconditional mean data of the previous sections from initial soot production though to downstream consumption, is a reflection of the predominance of rich mixtures upstream, giving way to lean mixtures downstream.

While the value of the peak conditional mean soot mass fractions increases down the length of the flame, the rate at which they increase, decreases with axial distance from the nozzle. This can be explained by the decrease in conditional mean temperature with axial distance that is associated with radiant heat loss (see Fig. 10). Those cases which have a higher temperature around the soot production composition over more of the flamelength tend to have a higher yield of soot. This is evident in the figure, where it is apparent that the conditional mean peak soot mass fraction for the low heat-loss low growth rate case *c5*, eventually exceeds the peak value of the higher growth rate case with high heat-loss (*c3*).

The influence of a reduced oxidation rate, present for case *c6*, can be seen in Fig. 8 where soot mass is not consumed to the same degree as the other cases and 'leaks' to lean mixture fractions. Notice also that the high heat loss cases (*c3* & *c4*) also display a small degree of leakage through the oxidation zone at the downstream locations where temperatures are so low as to retard oxidation.

The conditional mean particle molar abundance profiles in Fig. 9 are the product of two competing processes. Firstly, soot particles nucleate at rich mixture fractions where temperatures are high and soot precursors are plentiful. This composition appears to be in the vicinity of $\xi = 0.1$ in mixture fraction space. Secondly, the particles are modelled so that they agglomerate at all compositions at a rate which is proportional to the square of the number of particles present. It is apparent that in Fig. 9, that the particle abundance profiles are rapidly decaying from peak levels upstream to much lower levels downstream, as particle agglomeration occurs. The order of profiles from highest to lowest remains largely unchanged at all of the axial locations presented. The order of profiles from highest to lowest directly correlates with the order of conditional mean temperature profiles from highest to lowest. This would seem to suggest that in upstream regions where particles nucleate to the largest extent, the local temperature largely governs the resultant particle numbers.

The cases with similar high or low radiation adjustment factors display very similar conditional mean temperature profiles in Fig. 10. The spacing between the members of each profile group increases with axial distance as the differing levels of soot present cause different rates of heat loss. The effect of heat loss is to significantly reduce the peak conditional mean temperature in a monotonic fashion from the $x = 0.15$ plane through

Case No.	Radiation factor	Radiation model	Radiant fraction
c3	1.0	thin	0.58
c4	1.0	thin	0.60
c6	1.0	thin	0.60
c5	0.5	thin	0.43
c7	0.5	thin	0.42
s2	1.0	thick	0.32
s3	1.0	thick	0.32
s4	2.0	thick	0.34
s5	2.0	thick	0.34

Table 5: Comparison of flame radiant fractions predicted by different models. Note that case numbers correspond to those given in Tables 3 and 4.

to the end of the flame. There is no evidence of any relaxation of the conditional mean temperature profiles towards equilibrium at upstream locations, as was seen in an earlier study for hydrogen flames [1]. This is a testament to the strength of radiant emissions from hydrocarbon flames as modelled by optically-thin radiation heat transfer.

4 Discussion

The results presented in the above sections have shown the influence of varying the key soot kinetic rates for surface growth and oxidation, as well as the effect of arbitrarily modifying the magnitude of local heat loss. It has become apparent that the explicit description of the the four key soot-related processes within the soot model allows a good degree of flexibility in the parametric range of results.

While the results of the parametric variations have been instructive, it is clear that little can be achieved in the absence of an improved radiation model which can accurately account for heat transfer from flame media which is neither truly optically thick nor thin.

The difference in radiant heat transfer rate per unit length of flame for the current two radiation models is shown in Fig. 11. High and low radiation adjustment factor cases are shown for each model. It is evident that there is a large difference in precisely where energy is transferred from the flame as a whole, depending upon the model selected. In the case of the optically-thin model, heat loss from the flame appears greatest where the flame temperatures are the highest. For the optically-thick model, heat transfer from the flame is much more spatially even, with heat from the reaction zones being distributed throughout the flame by the radiant heat transfer. It is also apparent that there is no overall effect arising from applying a radiation adjustment factor to the Rosseland mean absorption coefficient of the optically-thick model. The adjustment merely serves to redistribute heat differently within the flame structure, while the overall output is unchanged.

The radiant fractions predicted by the various modelled cases for the flame of Nishida and Mukohara are given in Table 5. Radiant fraction is defined as the ratio of emitted

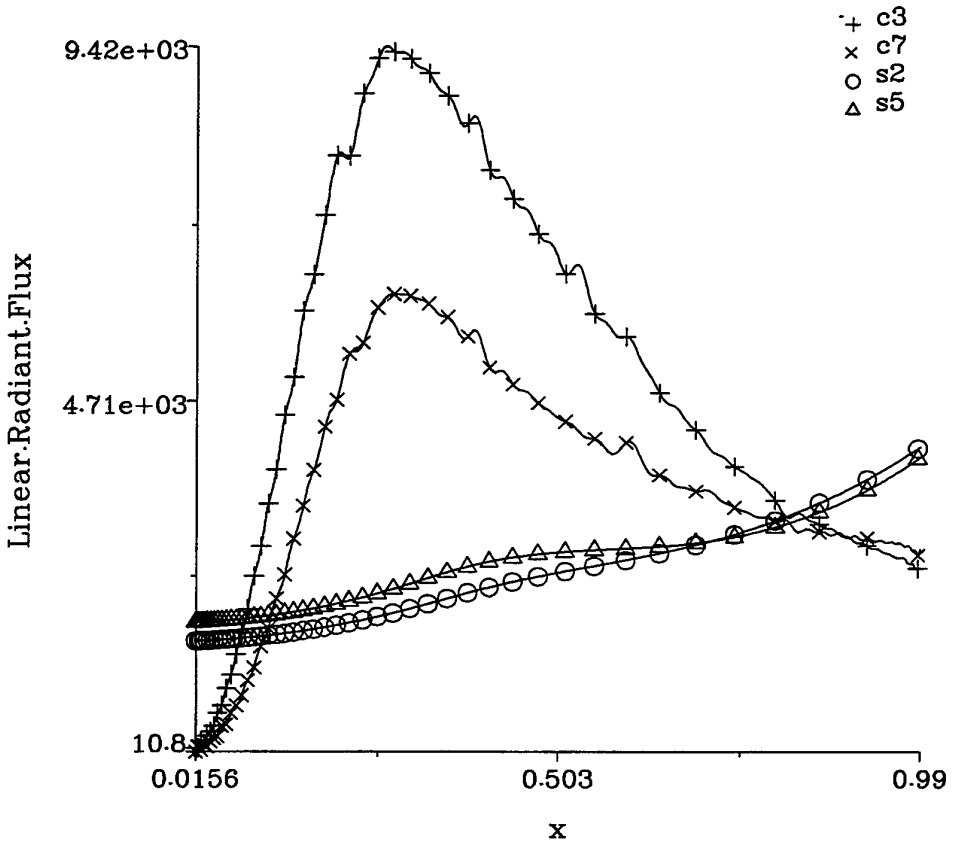

Figure 11: Axial profiles for linear radiant heat flux (in Watts per metre) predictions by the two models for different values of radiation factor. Legend designations correspond with entries in Tables 3 and 4.

energy to the energy evolved by the combustion of the fuel. The radiant fractions given in the table for the optically-thin CMC-soot calculations are unreasonably high. The values given for the optically-thick sootlet calculations are closer to an acceptable level for the nozzle size and flame power in question [30], however the form of the profile given in Fig. 11 is quite unlike what has been observed experimentally. The optically-thin profiles provide far better qualitative agreement.

The next stage in model development must neccesarily involve the incorporation of more advanced radiation heat transfer models which redress the shortcomings found in the predicted results. It is only then, that an effort can be made to find appropriate soot rate coefficients which can be taken to be reasonably universal. The coefficients devised by earlier researchers [5, 6, 10] using a 'fixed energy state' methodology (see Section 2.2.1) for flame prediction, have been found to be inappropriate when employed in conjunction with a radiation model. There is, however, every reason to expect that the soot model can be tuned for applicability in a wide range of sooting conditions given a reasonable heat transfer model. The earlier results of Leung and coworkers [5, 6] shows that reasonable agreement for soot levels can be found where predicted temperatures arbitrarily match that found in jet flames.

The great advantage of the radiation models employed in the models thus far, is that they entail very little computational expense over and above that involved in solving for the flame itself. A desirable aspect of any future sophisticated radiation model is that it should be as computationally inexpensive as possible while still providing reasonable confidence in its predictions.

Monte Carlo simulations of the full radiant heat transfer equations [31] provide a high degree of accuracy, flexibility, and fundamental significance. They are however, at this point, too computationally expensive and memory intensive to install within the TASCflow3D software suite. At the other end of the scale, the simple one-dimensional zonal flux method of Hottel and Sarofim [32] is computationally cheap but of limited use in modern combustor studies.

The so-called *discrete transfer* (DT) model of Lockwood and Shah [33] incorporates features of the full Monte Carlo solution technique as well as aspects of simpler flux models in a non-stochastic methodology. This method is the one which seems to warrant the closest attention, at this stage, for inclusion in a soot-capable predictive code. Stuttaford and Rubini [34], in particular, have developed the DT method to a stage where it can provide useful information of satisfactory accuracy.

The inclusion of the DT radiation model into the existing sootlet and CMC-soot models will be investigated in the immediate future. The CMC-soot model used in this study made use of geometric assumptions regarding uniformity of *conditional* mean reactive scalars across the flow which are known to apply in jet diffusion flames [29]. Applications involving the dilution flow in gas turbine combustors will involve a generalisation of this assumption to allow for radial variation in conditional mean reactive scalar statistics. Coincidentally, it is precisely this type of generalisation which is required in order to implement a DT radiation model within the CMC-soot model framework.

The sootlet model as it is currently implemented is well suited to the incorporation of the DT radiation model. Notable improvements which might reasonably be applied to the existing model include the abandonment of the *radiation factor* indexing of flamelet

libraries in favour of the more formal enthalpy deficit indexing described by Maracino and Lentini [35], and the addition of a tabulated mean fourth power of temperature in the soot-augmented flamelet library for use with the radiation model.

5 Conclusions

Two independent modelling strategies for predicting soot formation and its associated effects on radiant heat transfer in turbulent nonpremixed combustion have been described. The two model strategies share a representation of the global soot processes of nucleation, surface growth, oxidation and particle agglomeration.

Part of the description of the characteristic rates of soot formation and destruction involves an estimate of global chemical kinetic rate coefficients. As the rates being described are global approximations to what is actually a large set of elementary reactions, the estimation of these rate coefficients involves an unavoidable degree of empiricism.

The determination of a set of reasonably *universal* coefficients that can be used in both of the independent models has not been successful due to the inconsistent use of different models for radiation heat transfer in conjunction with the soot models. Further, the simplified radiation heat transfer models have been found to be not entirely appropriate for predictions in a luminous sooting environment.

The next stage of development involves the incorporation of a more advanced radiation heat transfer model into the existing combustion model framework. After this has been done, the process of finding appropriate soot rate coefficients can be allowed to proceed. The findings of a parametric study in soot model parameters indicate that sufficient flexibility exists to tune modelled rates, given a comprehensive set of comparative data and an accurate radiation model, to provide a reasonably universal soot prediction scheme.

A comprehensive data set for a range of conditions is being gathered from experiments at the time of writing.

References

1. Smith N. S. A.. 1997. *Comparison of CMC and SLF model predictions with experimental data for turbulent hydrogen jet flames.* DSTO Technical Report, DSTO-TR-0631, Aeronautical and Maritime Research Laboratory.

2. Nishida O., Mukohara S.. 1982. "Characteristics of Soot Formation and Decomposition in Turbulent Diffusion Flames." *Combustion and Flame*, v47, pp269-279.

3. Wagner H. Gg.. 1978. "Soot Formation in Combustion." *Seventeenth Symposium (International) on Combustion*, the Combustion Institute. pp3-22.

4. Frenklach M., Wang H.. 1990. "Detailed modelling of soot particle nucleation and growth." *Twenty-Third Symposium (International) on Combustion*, the Combustion Institute. p1559.

5. Leung K. M., Lindstedt R. P., Jones W. P.. 1991. "A Simplified Reaction Mechanism for Soot Formation in Nonpremixed Flames". *Combustion and Flame*, v87, pp289-305.

6. Fairweather M., Jones W.P., Ledin H.S., Lindstedt R.P.. 1992. "Predictions of soot formation in turbulent, non-premixed propane flames." *Twenty-Fourth Symposium (International) on Combustion*, The Combustion Institute. p1067-1074.

7. Bradley D., Dixon-Lewis G., El-Din Habik S., Mushi E.M.. 1984. "The oxidation of graphite powder in flame reaction zones." *Twentieth Symposium (International) on Combustion*, the Combustion Institute. p931.

8. Villasenor R., Kennedy I. M.. 1992. "Soot formation and oxidation in laminar diffusion flames". *Twenty-Fourth Symposium (International) on Combustion*, the Combustion Institute. pp1023-1030.

9. Neoh K.G., Howard J.B., Sarofim A.F.. 1984. "Effect of oxidation on the physical structure of soot." *Twentieth Symposium (International) on Combustion*, the Combustion Institute. pp951-957.

10. Kennedy I. M., Yam C., Rapp D. C., Santoro R. J.. 1996. "Modeling and Measurements of Soot and Species in a Laminar Diffusion Flame". *Combustion and Flame*, v107, pp368-382.

11. Peters N.. 1984. "Laminar diffusion flamelet models in nonpremixed turbulent combustion". *Progress in Energy and Combustion Science*, v10, pp319-339.

12. Peters N.. 1986. "Laminar Flamelet Concepts in Turbulent Combustion". *Twenty-First Symposium (International) on Combustion*, the Combustion Institute, Pittsburgh. pp1231-1250.

13. Smith N. S. A., 1994. *Development of the Conditional Moment Closure Method for Modelling Turbulent Combustion.* PhD Thesis, University of Sydney.

14. Smith N. S. A., Bilger R. W., Chen J.-Y.. 1992. "Modelling of Nonpremixed Hydrogen Jet Flames using a Conditional Moment Closure Method". *Twenty-Fourth Symposium (International) on Combustion*, the Combustion Institute. pp263-269.

15. Smith N. S. A., Bilger R. W., Carter C. D., Barlow R. S., Chen J.-Y.. 1995. "A Comparison of CMC and PDF Modelling Predictions with Experimental Nitric Oxide LIF/Raman Measurements in a Turbulent H2 Jet Flame". *Combustion Science and Technology*, v105, p357.

16. Girimaji S. S.. 1991. "Assumed Beta-pdf Model for Turbulent Mixing: Validation and Extension to Multiple Scalar Mixing". *Combustion Science and Technology*, v78, pp177-196.

17. Klimenko A. Yu., Bilger R. W.. 1992. "Relationship between conserved scalar pdfs and scalar dissipation in turbulent flows". *Charles Kolling Laboratory Report TNF-101*, University of Sydney.

18. Klimenko A. Yu.. 1990. "Multicomponent Diffusion of Various Admixtures in Turbulent Flow". *Fluid Dynamics*, v25, pp327-334.

19. Bilger R. W.. 1993. "Conditional Moment Methods for Turbulent Reacting Flow". *Physics of Fluids A*, v5, pp436-444.

20. Smith N. S. A., 1996. "Conditional Moment Closure of Mixing and Reaction in Turbulent Nonpremixed Combustion", *Annual Research Briefs* , Center for Turbulence Research. Stanford University / NASA Ames Research Center. pp85-100.

21. Li J. D., Bilger R. W.. 1993. "Measurement and Predictions of the Conditional Variance in a Turbulent Reactive-Scalar Mixing Layer". *Physics of Fluids*, v5, pp3255-3264.

22. Kronenburg A., Bilger R. W., Kent J. H.. 1997. "Second Order Conditional Moment Closure for Turbulent Jet Diffusion Flames". submitted to the *Twenty-Seventh Symposium (International) on Combustion.*

23. Smith N. S. A., 1998. "Modelling and Simulation of Particle Thermodynamics in Turbulent Flow". *Proceedings of the 1998 Summer Program*, Center for Turbulence Research, Stanford University / NASA Ames Research Center.

24. Siegel R., Howell J. R.. 1972. *Thermal Radiation Heat Transfer.* McGraw-Hill Book Company, New York.

25. Lee S.C., Tien C.L.. 1981. "Optical constants of soot in hydrocarbon flames." *Eighteenth Symposium (International) on Combustion*, the Combustion Institute, p1159.

26. Grosshandler W. L.. 1993. *RADCAL: A Narrow-Band Model for Radiation Calculations in a Combustion Environment.* NIST Technical Note 1402. National Institute of Standards and Technology. Gaithersburg, Maryland.

27. Advanced Scientific Computing. 1996. *TASCflow : Version 2.5.* Waterloo, Ontario, Canada.

28. Leung K. M., Lindstedt R. P., Jones W. P.. 1993. "Reduced Kinetic Mechanisms for Propane Diffusion Flames". in *Reduced Kinetic Mechanisms for Applications in Combustion Systems.* Peters N., Rogg B.. (eds). Springer-Verlag, Heidelberg. pp259-283.

29. Barlow R. S., Carter C. D.. 1996. "Relationships among Nitric Oxide, Temperature, and Mixture Fraction in Hydrogen Jet Flames". *Combustion and Flame*, v104, pp288-299.

30. Turns S. R. 1996. *An Introduction to Combustion*, McGraw-Hill Inc., New York.

31. Viskanta R., Menguc M. P.. 1987. "Radiation Heat Transfer in Combustion Systems". *Progress in Energy and Combustion Science*, v13, pp97-160.

32. Hottel H. C., Sarofim A. F.. 1967. *Radiative Transfer*, McGraw Hill, New York.

33. Lockwood F. C., Shah N. G.. 1987. "A New Radiation Solution Method for Incorporation in General Combustion Prediction Procedures". *Eighteenth Symposium (International) on Combustion.* The Combustion Institute, pp1405-1414.

34. Stuttaford P. J., Rubini P. A.. 1998. "Assessment of a Radiative Heat Transfer Model for Gas Turbine Combustor Preliminary Design". *Journal of Propulsion and Power*, v14, pp66-73.

35. Marracino B., Lentini D.. 1997. "Radiation Modelling in Non-Luminous Nonpremixed Turbulent Flames". *Combustion Science and Technology*, v128, pp23-48.

DISTRIBUTION LIST

Comparison of soot model predictions with experimental data for a turbulent sooting propane jet flame

Nigel S. A. Smith

	Number of Copies
AUSTRALIAN DEFENCE ORGANISATION	
S&T Program	
Chief Defence Scientist FAS Science Policy AS Science Corporate Management	1
Director General Science Policy Development	1
Counsellor Defence Science, London	Doc Data Sht
Counsellor Defence Science, Washington	Doc Data Sht
Scientific Adviser to MDRC Thailand	Doc Data Sht
Director General Scientific Advisers	1
Navy Scientific Adviser	Doc Data Sht
Scientific Adviser - Army	Doc Data Sht
Air Force Scientific Adviser	1
AMRL Personnel	
Director, Aeronautical and Maritime Research Laboratory	1
Chief, Airframes and Engines Division	1
Research Leader, Propulsion	1
Dr Simon Henbest (Functional Head), AED	1
Author : Dr Nigel S. A. Smith, AED	1
Dr J. Greg Bain, AED	1
Dr Kym Thalassoudis, WSD	1
Dr Farid Christo, WSD	1
DSTO Libraries	
Library, Fishermens Bend	1
Library, Maribyrnong	1
Library, Salisbury	2
Australian Archives	1
Library, MOD, Pyrmont	Doc Data Sht
Capability Development Division	
Director General Maritime Development	Doc Data Sht
Director General Land Development	Doc Data Sht

Director General C3I Development	Doc Data Sht
Army	
ABCA Office, G-1-34, Russell Offices, Canberra	4
SO (Science), DJFHQ(L), MILPO Enoggera	Doc Data Sht
NAPOC QWG Engineer NBCD	Doc Data Sht
Intelligence Program	
DGSTA Defence Intelligence Organisation	1
Corporate Support Program (libraries)	
OIC TRS, Defence Regional Library, Canberra	1
Officer in Charge, Document Exchange Centre (DEC)	1
Copies required by DEC for :	
US Defence Technical Information Center	2
UK Defence Research Information Centre	2
Canada Defence Scientific Information Service	1
NZ Defence Information Centre	1
National Library of Australia	1
UNIVERSITIES AND COLLEGES	
Australian Defence Force Academy	
Library	1
Head of Aerospace and Mechanical Engineering	1
Monash University	
Dr Damon Honnery, Dept. of Mechanical Engineering	1
Other Universities	
Deakin University Library, Serials Section (M list)	1
Senior Librarian, Hargrave Library, Monash University	1
Librarian, Flinders University	1
OTHER ORGANISATIONS	
NASA (Canberra)	1
AGPS	1
OVERSEAS	
Abstracting and Information Services	
Engineering Societies Library, US	1
Documents Librarian, The Center for Research Libraries, US	1

Information Exchange Agreement Partners

Acquisitions Unit, Science Reference and Information Service, UK	1
Library - Exchange Desk, National Institute of Standards and Technology, US	1

SPARES

Five copies	5

Total number of copies:	48

DEFENCE SCIENCE AND TECHNOLOGY ORGANISATION DOCUMENT CONTROL DATA				1. CAVEAT/PRIVACY MARKING
2. TITLE Comparison of soot model predictions with experimental data for a turbulent sooting propane jet flame			3. SECURITY CLASSIFICATION Document (U) Title (U) Abstract (U)	
4. AUTHOR(S) Nigel S. A. Smith			5. CORPORATE AUTHOR Aeronautical and Maritime Research Laboratory 506 Lorimer St, Fishermens Bend, Victoria, Australia 3207	
6a. DSTO NUMBER DSTO–TR–0676	6b. AR NUMBER AR-010-557		6c. TYPE OF REPORT Technical Report	7. DOCUMENT DATE August 1998
8. FILE NUMBER M1/9/502	9. TASK NUMBER DST 95/136	10. SPONSOR DSTO	11. No OF PAGES 40	12. No OF REFS 35
13. DOWNGRADING / DELIMITING INSTRUCTIONS Not Applicable			14. RELEASE AUTHORITY Chief, Airframes and Engines Division	

15. SECONDARY RELEASE STATEMENT OF THIS DOCUMENT

Approved For Public Release

OVERSEAS ENQUIRIES OUTSIDE STATED LIMITATIONS SHOULD BE REFERRED THROUGH DOCUMENT EXCHANGE CENTRE, DIS NETWORK OFFICE, DEPT OF DEFENCE, CAMPBELL PARK OFFICES, CANBERRA, ACT 2600

16. DELIBERATE ANNOUNCEMENT

No Limitations

17. CITATION IN OTHER DOCUMENTS

No Limitations

18. DEFTEST DESCRIPTORS

Soot
Combustion
Propane
Flames
Combustion deposits

19. ABSTRACT

Simplified global reaction steps for soot particle formation, growth, oxidation and agglomeration have been incorporated into two separate models for turbulent nonpremixed combustion. The first of these models is a hybrid steady laminar flamelet (SLF) model which uses flamelet library data to determine the local rates of the aforementioned soot processes at various rates of strain and degrees of radiant heat loss. The second model employs the soot processes in a Conditional Moment Closure (CMC) method and solves for soot mass fraction and particle abundance concurrently with the determination of gas phase reactions and radiant heat loss. The predictions of these two models are compared with experimental data for a turbulent propane jet flame. It is found that the interdependence between the rate of soot processes and radiation losses is an integral feature of the modelling problem. In general, it was not possible to determine a universally appropriate set of soot process rates, due to the need to take differences in radiation heat loss submodels and turbulent combustion models into account.